DEVELOPMENT OF A HYALURONIC ACID-BASED HYBRID BIOINK FOR STEREOLITHOGRAPHY 3D BIOPRINTING

by

Rafaeal Hossain Rakin

B.Sc. Electrical and Electronic Engineering,

North South University, Bangladesh, 2018

A THESIS SUBMITTED IN PARTIAL FULFILLMENT OF

THE REQUIREMENTS FOR THE DEGREE OF

MASTER OF APPLIED SCIENCE

in

THE COLLEGE OF GRADUATE STUDIES

(ELECTRICAL ENGINEERING)

THE UNIVERSITY OF BRITISH COLUMBIA

(Okanagan)

November 2020

The following individuals certify that they have read, and recommend to the College of Graduate Studies for acceptance, a thesis/dissertation entitled: Development of a Hyaluronic acid-Based Hybrid Bioink for Stereolithography 3D Bioprinting submitted by Rafaeal Hossain Rakin in partial fulfillment of the requirements of the degree of Master of Applied Science in Electrical Engineering.

Dr. Keekyoung Kim, Mechanical and Manufacturing Engineering, University of Calgary

Supervisor

Dr. Isaac Li, Irving K. Barber Faculty of Science, University of British Columbia

Co-Supervisor

Dr. Thomas Johnson, Faculty of Applied Science, University of British Columbia

Supervisory Committee Member

Dr. Zheng Liu, Faculty of Applied Science, University of British Columbia

Supervisory Committee Member

Dr. Jian Liu, Faculty of Applied Science, University of British Columbia

University Examiner

Abstract

In the near future, tissue engineering and 3D bioprinting techniques will be essential to alleviate the dire need for organs for transplantation. It promises a very automated, rapidly scalable, and patient-specific process that eradicates existing concerns. Therefore, there is an immediate need to develop biomaterials with intrinsic biological functionalities that can be used to mimic *In vivo* conditions. Hyaluronic acid (HA), being an extra-cellular matrix derivative, promises unique prospects in tissue-specific applications by virtue of its bioactive properties. The work presented in this thesis describes a tunable protocol for the synthesis of a dual-crosslinkable methacrylated hyaluronic acid (MeHA) with a high degree of substitution to be used as a bioink for Digital Light Processing Stereolithography (DLP-SLA) 3D bioprinting. Furthermore, to overcome the non-cell-adhesive nature of MeHA, a hybrid bioink in combination with gelatin methacryloyl (GelMA) is developed that can be used to produce 3D cell-laden hydrogel scaffolds. Upon development of the hybrid bioink, the mechanical properties, including microarchitecture, swelling ratio, and compressive modulus, were assessed along with its biocompatibility. The results show a 55% enhancement in mechanical strength compared to its sole constituents and enable cell-attachment in the presence of MeHA while maintaining high cell viability. Preliminary investigations also reveal that the hybrid bioink is a more suitable candidate for DLP-SLA 3D bioprinting compared to MeHA because of its printability and cell-adhesive properties. Although, further optimization of the printing process with the hybrid bioink and the specific influences of MeHA on specialized cell types is required to be understood. This thesis lays out a firm foundation for the development of a stable MeHA bioink for DLA-SLA 3D bioprinting. It offers solutions to overcome its major limitations, without complex chemical modifications, by developing a hybrid hydrogel bioink.

Lay Summary

The dire need for organs and its consequent shortage worldwide is a problem that requires immediate attention as the need intensifies each day. Tissue engineering techniques combined with additive manufacturing technologies could help resolve this problem through 3D bioprinting. It could potentially enable the development of lab-made organs for transplantation and research. Therefore, there is a growing need to develop biomaterials that can resemble native conditions for biological cells. Hyaluronic acid (HA) has wound-healing and inflammation-reducing capabilities and is a substance found abundantly in the human body. The work presented in this thesis modifies HA to be photocrosslinkable so that it can transition from liquid to gel with exposure to visible light hence be compatible with the Digital Light Processing Stereolithography (DLP-SLA)-based 3D bioprinting system. Moreover, to overcome some major limitations posed by photocrosslinkable HA, it is combined with photocrosslinkable gelatin to produce a mechanically enhanced, cell-adhesive, and photocrosslinkable bioink.

Preface

The investigations presented in this thesis are the original work of the author and were conducted under the supervision of Dr. Keekyoung Kim and Dr. Isaac Li in the Advanced Biofabrication Laboratory, School of Engineering at the University of British Columbia, Okanagan.

The following parts of the thesis have been published:

Parts of chapter 1 and chapter 5 have been published in:

P. Ambhorkar*, **R.H. Rakin***, Z. Wang*, H. Kumar, and K. Kim, "Biofabrication strategies for engineering heterogeneous artificial tissues", Additive Manufacturing, vol. 36, p. 101459, 2020. Available: 10.1016/j.addma.2020.101459.

Manuscripts Under Preparation

Chapters 2, 3, and 4 will be used towards preparing: **R.H., Rakin**, H. Kumar, F. Menard, I.T.S. Li & K. Kim, “The Development of a cell-adhesive hybrid bioink with Gelatin methacryloyl and Methacrylated Hyaluronic acid for DLP Stereolithography 3D Bioprinting”

Table of Contents

List of Tables

List of Abbreviations

ADSCs	Adipose-Derived Stem Cells
DLP	Digital Light Processing
DMD	Digital Micromirror Device
DMF	Dimethylformamide
DS	Degree of substitution
ECM	Extracellular Matrix
EDTA	Ethylenediaminetetraacetic acid
EY	Eosin-Y
FRESH	Freeform Reversible Embedding of Suspended Hydrogels
GelMA	Gelatin methacrylate
GM	Glycidyl methacrylate
GSC	Glial Stem Cells
HA	Hyaluronic acid
HBdSMC	Human Bladder Smooth Muscle Cells
HNDF	Human neonatal dermal fibroblasts
HUC	Human Urothelial Cells
HUVEC	Human Umbilical Vascular Endothelial Cell
MeHA	Methacrylated hyaluronic acid
PBS	Phosphate buffer saline
PCL	Polycaprolactone
qPCR	Real-time polymerase chain reaction
PEGDA	Polyethylene glycol diacrylate

RGD	Arginine-Glycine-Aspartate
RO	Reverse osmosis
RPM	Rotations per minute
SLA	Stereolithography
TEA	Triethylamine
TEOA	Triethanolamine
UV	Ultraviolet radiation

List of Figures

Acknowledgements

First and foremost, my sincere gratitude goes out to my supervisors, Dr. Keekyoung Kim and Dr. Isaac Li for their support and guidance. I am also thankful to my supervisory committee members, Dr. Zheng Liu, Dr. Thomas Johnson, and Dr. Jian Liu for their support along the way.

I will always be thankful to Dr. Kim for this opportunity and for introducing me to this field of research. Graduate research was only more rewarding because of his guidance and the freedom that he gave me to explore, learn, and enjoy research. Likewise, I will always be indebted to Dr. Li for taking me in and guiding me through the most difficult period in the program. He has always helped me navigate the most difficult problems and greatly facilitated my growth in research. I, also, must not forget to thank Dr. Fredrick Menard for his invaluable insights on my projects. I will always fondly remember the drop-in chemistry-recaps, brainstorming sessions, and emergency reagent pickups that helped me tremendously.

In the past years, I have learned the most from my colleagues at the Advanced Biofabrication and The Single Molecule Mechanobiology Lab. I am thankful to each and everyone for their expertise, time, and help. However, there are a few who deserve a special mention.

The first among them, Hitendra Kumar. I would not go on to complete my research project without his persistent efforts in training and mentoring me. I cannot be thankful enough for the countless hours discussing the many project ideas, designing experiments, and most importantly, the instant SOS calls on WhatsApp. I am truly inspired by his humility, work ethic, and ingenuity. My gratitude would go out to Dr. Kabilan Sakthivel for his support in various capacities in the lab including cell-culture, imaging and mechanobiology. Mechanical characterization of my samples would not be possible without Mahmoud Sakr. His many expertise and support especially towards the end of the project were crucial to my progress. The list would not be complete without Pranav Ambhorkar. I will always remember the many insightful discussions and his support which helped me settle in and got me acquainted with the laws of the lab.

Lastly, I must express my utmost gratitude to all my teachers in the past 18 years of education and especially, Dr. Subir C. Ghosh for inspiring me to take on this journey and pursue graduate studies. Without the guidance and love of my teachers, I would not be where I am today.

Dedication

In the name of Allah, the Most Gracious, the Most Merciful.

For my mother, father, sisters - Oyshe & Elma, and Noshin

you are my reason and strength.

"And when My servants ask you, [O Muhammad], concerning Me - indeed I am near. I respond to the invocation of the supplicant when he calls upon Me. So let them respond to Me [by obedience] and believe in Me that they may be [rightly] guided." - 2:186, The Holy Quran.

Chapter 1: Introduction

Over the last decade, the shortage of organs has become increasingly prevalent globally in developed and developing nations alike. According to statistics reported by the U.S Department of Health and Human Services, as of January 2019, more than 113,000 people were on the waiting list for a life-saving organ, meanwhile, only 36, 528 organ transplant procedures were conducted in the year 2018 [1]. The report also mentions that an alarming up to 20 people die every day as they wait for an organ. The deficit of organs, as demonstrated by these statistics is unlikely to be resolved solely by organ donation and it is becoming increasingly clear that an alternative solution is of dire need. Research into developing artificial tissues and organs using tissue-engineering techniques has gained much prominence in this very context and has served to be a promising solution for the growing organ shortage [2]. To date, several organs have been engineered artificially and implanted *In vivo* including; the trachea [3], the lung [4], and the urinary bladder [5]. Artificial 3D tissue models have also become very popular for use as platforms for drug discovery and disease modeling [6]. These tissue-engineered models mimic the *In vivo* 3D cellular microenvironments more accurately as compared to their vastly oversimplified 2D counterparts and inaccurate animal models, while at the same time also offering high observability and ease of data visualization [7]. Some examples of tissue and disease models that have been established by tissue engineering include; the kidney [8], kidney disease [9], cancer tumor [10], lung [11], and the skin [12].

The generation of engineered tissues is a step-by-step process that can typically be realized through the following workflow (See Figure 1.1): (1) The isolation of various autologous target cells or stem cells from the human body; (2) The proliferation of cells (and differentiation in the case of stem cells) to yield large cell-populations; (3) The application of a biofabrication process

to combine the different cells and biomaterials to create temporary heterogeneous tissue scaffolds; (4) Supplementary culturing of cells on the 3D scaffolds to form artificial tissues; and (5) The implementation of these artificial tissues as either, implants *In vivo* or as models for studying diseases *in-vitro.* Within this workflow, the step comprising of the biofabrication process is arguably the most critical process since it directs the precise alignment and placement of cells and biomaterials, which in turn governs the adequate functioning of the engineered tissue. For this reason, the specific biofabrication process used for generating tissue microenvironments is also crucial in determining their feasibility and functionality [13]. Biofabrication has been defined as *"the automated generation of biologically functional products with structural organization from living cells, bioactive molecules, biomaterials, cell aggregates, through bioprinting or bioassembly and subsequent tissue maturation processes"* [14]. Biofabrication techniques can be divided into two classes of approaches; top-down and bottom-up. Top-down methods are considered to be those where cells are traditionally seeded onto fabricated whole sized scaffolds and then matured; meanwhile, bottom-up approaches involve the assembly of modular microtissues to form microtissues, however, the separation between the two approaches is not clear [15,16]. Figure 1.2 elucidates the differences between top-down and bottom-up methods in more detail. Analogous to nanofabrication, top-down biofabrication methods are more direct, controllable, and faster, while bottom-up methods tend to be more precise [17].

Both top-down and bottom-up approaches have been used widely, for the successful generation of artificial tissues including blood vessels [16-18], cardiac tissue [19-21], cartilage [22,23], skin [24], tumor [25], neural tissue [26] , adipose tissue [27] and stem cell microenvironments [28,29]. Most of these artificial tissues are created from a single cell-type. However, most tissues existing *In vivo* do not function independently from each other. For

instance, blood capillaries, which are essentially a result of vascular endothelial cells being arranged in the form of a vessel, are distributed in every tissue of the human body and are responsible for ensuring the exchange of oxygen, nutrition, and biomolecules. Without this circulatory network, cells and in turn tissues cannot survive [30]. Therefore, to fabricate functional artificial tissues and organs, the integration of multiple cell types is necessary. Furthermore, compatible biomaterials must be employed for scaffold creation while an anatomically realistic distribution of cells that closely mimics the cellular microenvironment must be sought in order to ensure the viability of such constructs.

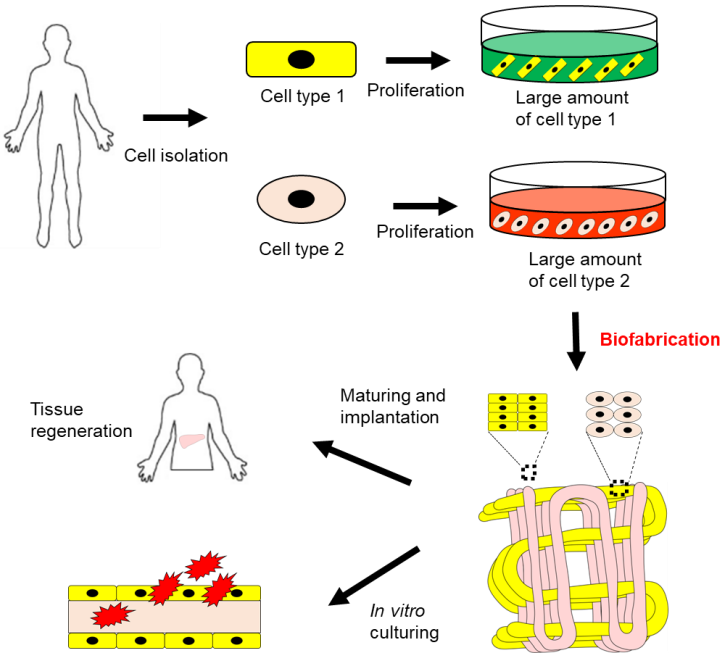

Figure 1.1. The typical workflow for fabricating heterogeneous artificial tissues used in tissue regeneration and disease study. The workflow involves steps as follows: 1. Isolation of cells from the human body 2. Cell proliferation and differentiation to yield large populations of specific cells 3. Biofabrication process that can assemble multiple-cells and biomaterials onto heterogeneous tissue scaffolds 4. The application of heterogeneous tissue scaffolds for tissue regeneration and disease study. (Adopted from [31])

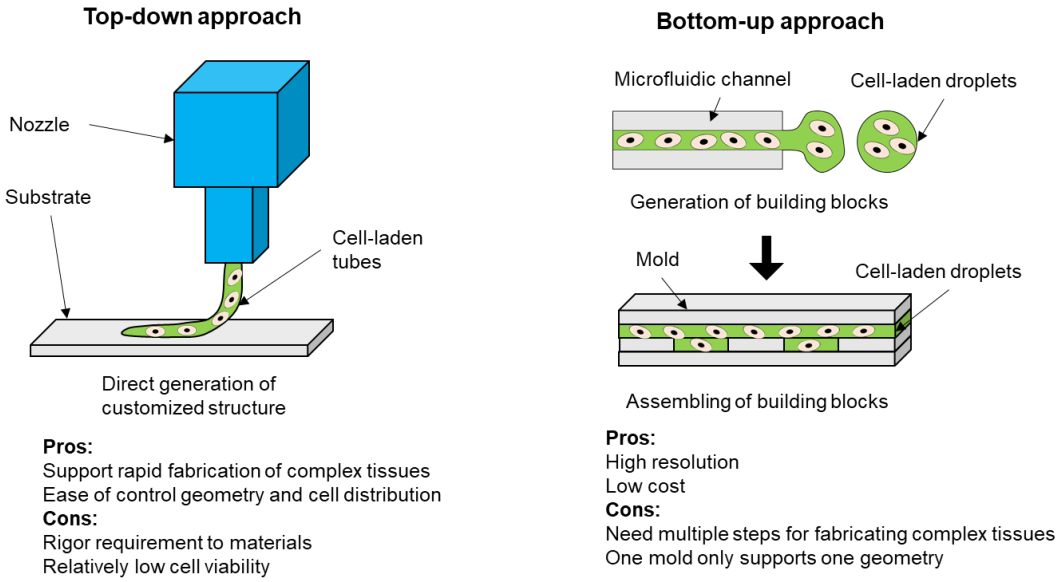

Figure 1.2. Top-down and Bottom-up approaches for biofabrication. The top-down approach aims to fabricate desired heterogeneous tissues directly through bioprinting. On the other hand, the bottom-up approach is a multi-step fabrication process, where the pre-generated building blocks are assembled to construct desired tissues. (Adopted from [31])

1.1 Advanced Biofabrication Strategies

The top-down approach in biofabrication is sought after due to its ease and automated control over scaffold development. The ability to fabricate and crosslink multi-material scaffolds layer-by-layer with this approach aids greatly in developing heterogeneous tissues [32]. Contrary to the top-down approach, bottom-up methods seek first to generate micro-sized cellular constructs to act as building blocks, which could then be assembled for developing complex structures. Bottom-up approaches can be described as a two-step fabrication process that consists first of the creation of these building block units, followed by their eventual assembly. The cellular constructs used as building units for this purpose can be categorized further as belonging to one of three standardized

shapes; points, lines, and planes [33]. This section discusses popular techniques based on the top-down approach, including: inkjet, extrusion, and stereolithography (SLA) bioprinting.

1.1.1 Inkjet Bioprinting

Inkjet bioprinting is very similar to traditional inkjet printing with respect to its working principle. This has rendered it substantially easier to translate the well-known dispensing technology into bioprinting related applications. Due to their simplicity and ease of operating, inkjet bioprinters are known for producing precision and high-throughput complex heterogeneous tissues at a low and affordable cost. Inkjet printing systems perform efficiently in patterning multicellular high-resolution scaffolds with multiple layers, which saw its application in printing vascular models, skin tissues, and others[34].

Xu *et al*. pioneered inkjet-based bioprinting in 2005 and demonstrated the production of scaffolds from digital images by injecting droplet ink on substrates [35,36]. Drop-on-demand inkjet bioprinters dispense a bioink—a mixture of biocompatible media and cells—from a storage cartridge through a print head through various mechanisms. Some widely used inkjet bioprinting mechanisms are based on thermal, piezoelectric, electrostatic, and electrohydrodynamic properties. Piezoelectric inkjet bioprinters use piezoelectric crystals for generating mechanical stimuli from electrical signals to dispense the bioink as a droplet. Likewise, thermal inkjet printers use thermal actuators and micro-resists to generate necessary heat for bioink expansion, bubble formation, and deposition. Electrostatic inkjet printers deploy simple mechanical actuators for dispensing bioinks as the droplet is guided using an electrostatic field. Likewise, some printers use large potential differences, usually 0.5-20 kV, for dispensing distinct droplets on the substrate [35]. In 2016 Bsoul *et al.* [37] demonstrated the successful integration of a microfluidic mixer print

head, using which a variety of bioinks could be mixed within a single droplet before deposition. More recently, Sakai *et al*. demonstrated multi-material printing by dispensing multiple bioinks through a piezoelectric printer. This device was able to dispense two different bioinks, whose crosslinking macromolecules by using horseradish peroxidase and hydrogen peroxide, which has been reported to have high cell viability and cytocompatibility [38]. In addition to combining multiple bioinks and to further enable multi-material printing, researchers have also attempted to hybridize inkjet technologies. For instance, Yoon *et al.* [39] combined spray-coating with piezoelectric bioprinting for enabling the production of high resolution and free form large-scale, cell-laden hydrogel scaffolds by successfully modifying the drop-on-demand method. Subsequently, hydrogels of diverse material compositions, including alginate, gelatin methacryloyl (GelMA), fibrinogen, and cellulose nanofiber, were printed in various shapes, thus demonstrating the immense potential of inkjet bioprinting in dispensing multiple materials to print complex structures. However, the discontinuity of droplets and the exposure of cells to high temperatures and voltages that is characteristic of inkjet-based technologies can lead to cell-damage remains a major concern that needs to be addressed in future research.

1.1.2 Extrusion Bioprinting

In extrusion bioprinting, the print head cartridge used in inkjet bioprinting is replaced with pneumatic actuators and nozzles. This makes it possible to extrude defined volumes or strips of bioinks onto the substrate. The extruded biomaterials can then be crosslinked to form scaffolds via a light or a chemical-based crosslinking process. Therefore, the construction of complex structures utilizing extrusion mechanisms can be used to bioprint complex tissues include hepatic lobule, capillaries, cardiac patches, etc. Figure 1.3 (B) illustrates the method of extrusion, which depends

on some major factors including (1) nozzle diameter, (2) rate of extrusion (3) speed of printer head (4) biomaterial viscosity, and (5) temperature of the nozzle to determine the scaffold fabrication quality [40].

Existing extrusion systems range from shear-thinning deposition to coagulation and support baths. However, there are several approaches taken to modify these deposition techniques. Adopting and evolving from coagulation baths, co-axial extrusion offers another solution. Simultaneous delivery of the bioink and the crosslinker at the nozzle tip allow for forming core-shell constructs. Also, the integration of microfluidic devices with printer heads enables multi-material printing and on-demand change of bioinks by virtue of its capability to hold multiple bioinks at any instant[41,42]. Hence, it is possible to create diverse extracellular matrix (ECM) environments for the cells with consistency and repeatability. Depending on the arrangement of the bioink and crosslinking agent inside the co-axial nozzle, such an extrusion system allows for the printing of bulk and hollow core-shell structures made of several different materials, including GelMA and alginate, which could serve as a key tool to for solving complications relating to vascularization in fabricated heterogeneous tissues[41,43]. Liu *et al.* demonstrated co-axial extrusion using GelMA and alginate, thus overcoming the limitation of fabricating functioning cell-laden soft constructs from low-concentration bioinks [44]. Also, Ouyang *et al*. illustrated a 3D bioprinting method which crosslinks the bioink *in-situ* in the nozzle during the printing process before deposition [45]. The group well demonstrated the printing of uniform and consistent structures using photo-permeable nozzles and a variety of hydrogels, including GelMA, methacrylated hyaluronic acid (MeHA), poly(ethylene glycol) diacrylate (PEGDA), and norbornene-functionalized hyaluronic acid (NorHA). Resolutions as fine as 60-700μm filaments were attainable depending on the capillary dimensions. Moreover, controllable heterogeneous core

shell structures were also formed during the experiment while maintaining high cell viability which allows for great scope in heterogeneous tissue fabrication.

Beyond co-axial extrusion, it is possible to alter the shape of the constructs during extrusion printing, as demonstrated by Kang *et al.* using pre-set extrusion nozzles [46]. They have enabled multi-material bioprinting via a multilateral loaded precursor bioink cartridge in a pre-defined shape to be extruded by a syringe-based print head. This may even make it possible to use several struts to fabricate large-scale tissues. The cell viability of a co-culture using hepatocellular carcinoma cells (HepG2) and endothelial cells (EC) in the shape of a hepatic lobule made using this technique has shown more than 90% viability after 5 days. It is also possible to use change extrusion dynamics to enable different printing methodologies using just one nozzle. In 2018, Yuk and Zhao demonstrated a new Direct Ink Writing printing with a single nozzle by intentional stretching and accretion of the extruded ink [47]. The group shows the ability of single nozzle systems to produce scaffolds with resolution finer than the nozzle diameter that can produce continuous, non-continuous, and complex structures with the simple motion of the one nozzle.

For instance, the brain is one of the most extensively studied organs in tissue engineering. The complex nature of various neurodegenerative diseases and the lack of accessibility to the brain *in vivo* has attracted several researchers to develop analogous brain tissue and blood-brain-barrier models. Bioprinting plays a pivotal role in the development of such models. Over the years, various simplified and complex brain tissue models have been proposed [48,49]. More emphasis is laid on these models' functional complexity, which arises from the requirement of multiple constituent cell types. However, the role of structural complexity in brain tissue engineering has not caught the same level of attention due to its highly indirect nature of influence [50]. In 2015, Lozano *et al.* used a handheld coaxial nozzle extrusion system to fabricate a multi-layered brain tissue [51].

Gellan gum modified with Arginine, Glycine, and Aspartate (RGD) peptides was used as the biomaterial to encapsulate cortical neurons. Although this model lacked the mix of constituent cell types and utilized a single type of cell, it provided valuable insights into the growth of neuron processes towards the neurons in the vicinity by crossing a cell-free biomaterial zone. In another recent study, a multistep bioprinting approach was used to fabricate a glioblastoma tumour model [52]. The authors printed collagen layers as substrates and perfusable channels with gelatin as sacrificial material. Two essential cell types were used in the fabricated structure – glioblastoma and human umbilical cord vein endothelial cells (HUVECs). Using this tumour model, the authors presented the influence of drugs delivered through the vascular channels over long-term culture.

Like the brain, heart tissue engineering has also been an attractive theme of research in which the role of bioprinting has been indispensable. Various types of electrically conductive biomaterials have found their application in the development of cardiac patches. Shin *et al.* and Zhu *et al.* used gelatin methacrylate combined with reduced graphene oxide and gold nanoparticles to fabricate electrically conductive cardiac patches using the extrusion bioprinting method [53,54]. Owing to the electrically conductive property of these patches, the cardiomyocytes were observed to proliferate faster with higher cell viability. In more recent work, Noor *et al.* reported the bioprinting of thick perfusable cardiac patches and a miniaturized vascular heart structure [55]. Although the vasculature was simplified, this work caught worldwide attention by replicating the structural complexity of the heart along with the integration of induced pluripotent stem cells (iPSC) derived cardiomyocytes and human neonatal dermal fibroblasts (HNDF). The authors used an extrusion bioprinting approach to fabricate cardiac patches. For the bioprinting of the heart, the extrusion method was used in conjunction with a support gel bath. This bioprinting approach has been reported as a freeform reversible embedding of suspended hydrogels (FRESH) [56]. In 2019,

Lee *et al.* used the FRESH bioprinting approach to fabricate heart structure with human cardiomyocytes [57]. The authors demonstrated the fabrication of free-standing structures with integrated vasculature. These two studies also presented how an evolved extrusion method contributed to achieving significant improvement in printing both structurally and compositionally complex tissue constructs.

Extrusion bioprinting can form 3D scaffolds with desired precision and heterogeneity. However, due to the large external forces applied to the cells during the extrusion, the cell viability is relatively low after fabrication [44]. Few concerns regarding extrusion-bioprinting lie in printing parameters, material compatibility, cell viability, and the printability of materials [40]. Although extrusion bioprinting offers a much faster printing time, this could be a tradeoff with low cell viability. Since scaffolds are usually printed layer-by-layer, outside of cell culture conditions, cell viability is negatively affected [40].

1.1.3 Stereolithography (SLA) Bioprinting

Often regarded as a freeform printing process, SLA allows for more liberty in design and printing when compared to its contemporaries. It removes much of the complexity that comes with requirements like fabricated moulds and precursor cartridges. In this method, a digital image of the structure is sliced into layers, which are then projected onto a photo-crosslinkable polymer or hydrogel substrate [58]. As only the exposed area on the substrate is crosslinked, layer-by-layer solidification of the substrate can be carried out until the desired 3D structure is complete. The light, often visible or UV from sources including simple computer projectors, focused laser beams, and digital micromirror arrays can be used to pattern a substrate [59–62]. The process of stereolithography is illustrated in Figure 1.3.

SLA can print whole layers at once, whereas both its contemporaries are only able to print single points and coordinates, as a result, it has the fastest printing speed. Moreover, the non-contact printing method does not have an adverse influence of shear stress on the cells, due to which the cell viability is significantly higher. The resolution of the scaffold, however, is reliant on the lens or illumination system, which is as good as 5 μm [63]. Miri *et al*. have demonstrated the use of a mask-free SLA approach with the aid of a digital micromirror and a microfluidic device for fabricating a 3D heterogeneous construct [64]. The microfluidic device, possessing a pneumatic valve, enables the switching between different bioinks that are crosslinked layer-by-layer with UV. Once a layer is crosslinked, the remaining bioink is washed away with phosphate-buffered saline (PBS) and this is repeated until the whole structure is printed. The device demonstrated the printing of high spatial resolution of 3D constructs from multiple hydrogels including PEGDA and GelMA. The possibility of using GelMA with SLA for biofabrication was also illustrated by Wang and Kumar *et al.* The diverse 3D hydrogel scaffold developed by the group, showed high cell viability and in a 3D network [65]. However, the physical size of the constructs is limited to the microfluidic device and the process is quite labor-intensive. Utilizing a digital light projection (DLP) based printing system, Ma *et al.* reported the fabrication of cirrhotic liver tissue using a decellularized extracellular matrix and HepG2 cells [66]. Their proposed methodology implemented a light-based bioprinting system to produce a 3D scaffold that could mimic the mechanical and microarchitectural properties of cirrhotic liver tissue. The study used biocompatible and native biomaterials for the printing process, for this reason, it could easily be used for disease modeling or drug screening applications.

Similarly, using a SLA printing system, Yu and their group has been able to print pre-vascularized scaffolds that host HUVECs and clonal mouse embryo (10T1/2) cells to work as a

biomimetic model of the hepatic tissue [67]. The group used a combination of naturally derived bioinks like gelatin methacrylate and methacrylated hyaluronic acid to ensure a biocompatible environment. Upon examination, the hepatic tissue models show the adaptation of phenotypic behavior by 10T1/2 cells and lumen-like structure formation by the HUVECs in a week. Furthermore, Yu *et al*. conducted an *In vivo* study of their pre-vascularized model in immuno-deficient mice which showed that their hepatic model containing human induced Pluripotent Stem Cells (hiPSC) derived hepatic progenitor cells (hiPSC-HPCs), HUVECs**,** and human adipose-derived stem cells **(**ADSCs**)** had enhanced development of the vasculature with red blood cells present within them. Moreover, immunohistochemical staining results of albumin and E-cadherin, exhibit aggregation and spheroid formation in the scaffold.

Recently, Ali *et al.* demonstrated the methacrylation of porcine kidney-derived extra-cellular matrix (ECM) (kdECMMA) making it photocrosslinkable [68]. Since this bioink was sourced from the kidney, the group hypothesized that the presence of kidney-specific biomolecules would aid in the fabrication of more accurate renal structures. The study also revealed positive results regarding the organization of the bioprinted kidney cells towards forming tubular structures, indicating the potential to form intricate renal structures like the glomerular unit.

Last year, Bernal *et al*. demonstrated a revolutionary volumetric bioprinting technique that seeks to fabricate a complex 3D free-floating structures made of photocrosslinkable gelatin hydrogels [69]. With this technique, whole structures can be developed at a time in a matter of seconds without the need for the addition of multiple layers thus making the bioprinting process more scalable.

Despite its advantages, one limitation of SLA bioprinting is that the process is only compatible with substrates that are photo-crosslinkable. Most importantly, for multi-material

printing applications, managing contamination is crucial— along with material choice and compatibility.

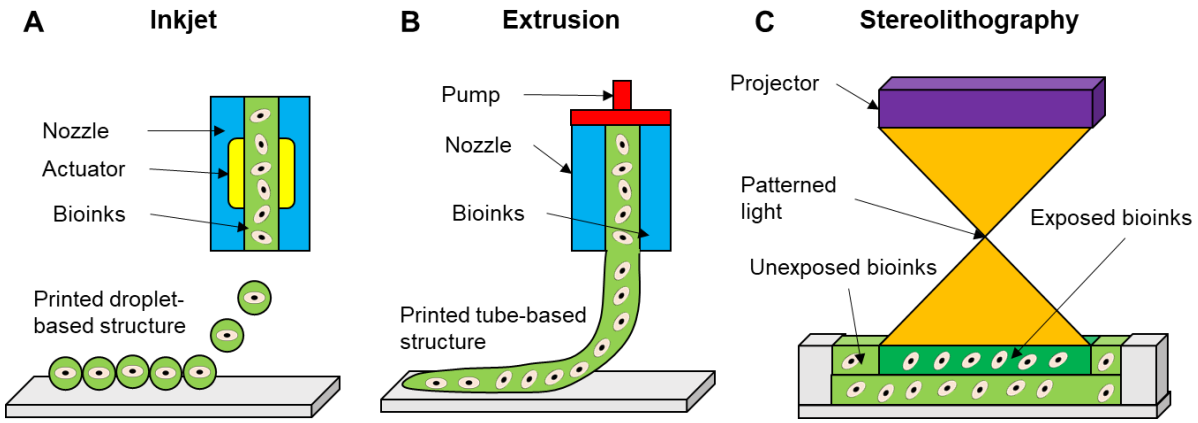

Figure 1.3. Working principles of bioprinting approaches (A) Inkjet bioprinting: A piezoelectric actuator ejects discontinuous droplets to form tissue structures (B) Extrusion bioprinting: A pump applies a continuous external force to extrude out tubes for tissue scaffolds. (Adopted from [31])

1.2 Bioinks in 3D bioprinting

Additive manufacturing techniques like 3D printing which is the overarching technology for 3D bioprinting – rely heavily on the use of raw materials that make the 3D scaffold. The resin used in a conventional 3D printer is replaced with a "bioink" – a material that can sustain living cell units inside the 3D conduit. One of the important components of 3D bioprinting is the bioink that is used for the printing. This bioink should be highly biocompatible to accommodate live-cell and mechanically stable after printing. It should also provide high resolution during printing. Hydrogels are the most prominent materials which are used as bioink in 3D bioprinting. However, for a material to be selected as a bioink, they need to fulfill the requirements discussed below:

Biocompatibility: Biocompatibility refers to the biological requirements and properties posed by the bioink. It means that the bioink material should not only be non-toxic but it should also ensure the viability of live cells, cytocompatibility, and bioactivity of cells after printing. The boink material, should not influence any adverse immunological response to the host when it is *In vivo*. Moreover, it should be able to facilitate cell attachment, growth, and proliferation inside the 3D construct and it should be convenient to modify the bioink molecule to enable different biochemical signals.

Physical properties: The viscosity of the bioink should, in principle, be tunable depending on the application. In order to facilitate the usage of the same bioink with different available 3D bioprinting techniques, the viscosity needs to be manageable. In addition, the printed scaffolds need to retain their shape post-printing for a definite time period. Hence, the materials should have some degree of stiffness so that it maintains mechanical integrity while also supporting cellular behavior modulated by stiffness. The biodegradation of the selected biomaterial should match with that of the tissue of interest, so that once the cells grow and proliferate, eventually they can replace the biodegrading construct with their own regenerated ECMs

Nutrient permeability: The cells or tissues encapsulated in the bioink should remain viable post-printing. The supply of nutrients in the scaffold is key to cell viability, therefore, the bioink material must show permeability to oxygen gas and other nutrients. Alongside this, its transport of metabolic cell wastes should also be considered.

Printability: It is crucial to understand the processing capabilities of the bioink to understand the printability of the material. To be compatible with 3D bioprinting, the bioink materials should be able to retain its shape by itself post-printing. This characteristic and the overall printability is a combination of multiple factors, hand-in-hand, that play an important role in determining the

printability. Parameters such as viscosity, surface tension, crosslinkability, and surface properties are key to determine printability.

The other important desirable aspects for a bioink include high resolution during printing, in situ gelations, visco-elastic properties, low cost, readily available, industrial scalability, biomimicking the tissue internal structures, mechanical integrity, short post-printing time for maturation, and immunological compatibility.

1.2.1 Natural Bioinks

The goal of 3D bioprinting is to ensure and provide a 3-dimensional biomimetic environment for the biological units. In order to ensure a proper biomimetic environment, using natural derivatives is the most desirable option. That is why the use of hydrogel from natural sources is most common in all applications because it increases the chances of a biocompatible environment with no or very low adverse impact on the cells. Cells hosted within the hydrogel matrix during bioprinting must be in a viable environment that is biocompatible and allows the exchange of necessary nutrients. Ideally, the hydrogel should not trigger any immunological reaction and have an optimal degradation rate to allow the cells to protect and allow the cells to proliferate within the matrix. Hydrogel derived from natural sources contain macro and micromolecules which can offer an environment that is most similar to native microenvironments. Some natural hydrogel is derived from the extracellular matrix of living hosts which makes them very biocompatible with more functionalities. Overall, natural hydrogels have the properties that enable biocompatibility, functionality, permeability to necessary nutrients, along with the required chemical structure and functionality demanded by bioprinting processes [70].

Gelatin and Gelatin Methacryloyl (GelMA): Gelatin is a collagen-based natural hydrogel and is widely used as a bioink. Obtained primarily from bones and tissues of animals like fishes and pigs, this form of collagen can form gels at low temperatures which is reversible to liquid at the higher temperatures. Moreover, it is known to retain the amine groups from collagen as a result it aids in cell adhesion, proliferation, and differentiation[71]. Implementation of various crosslinking methods for gelatin has already been explored including chemical crosslinking with the likes of transglutaminase [83] horseradish peroxidase (HRP) and hydrogen peroxide (H2O2) [82] and photocrosslinking of methacrylate modified gelatin with 2-hydroxy-4′-(2-hydroxyethoxy)-2-methylpropiophenone (Irgacure 2959), lithium-phenyl-2,4,6-trimethylbenzoyl-phosphinate(LAP)2,2'-azobis[2-methyl-N(2hydroxyethyl)-propionamide] (VA-086). Although elongation of cells within the hydrogel is restricted due to decreased RGD groups, however, pristine gelatin hydrogel but can keep cells viable over long periods [72]. Moreover, scaffolds fabricated with only gelatin do not show good mechanical properties despite that they have been used in all types of bioprinting systems. For an instance, Wang *et al*. used an extrusion-based bioprinting system to print and encapsulate hepatocytes which retained its viability within the matrix for over 2 months [73]. In 2007, droplet-based bioprinting was used by Boland *et al*. with a hybrid of gelatin and alginate[74]. The study encapsulated endothelial cells and printed structures up to 1cm in thickness with high cell viability. Laser-based systems were also used to bioprint with gelatin which ensured cell stable and biocompatible matrix without minimal damage to cell during printing [75]

Modifying gelatin with methacrylate groups to be used as a bioink is probably one of the most seen applications is naturally derived gelatin-based hydrogels. The naturally available denatured collagen – gelatin is modified with methacrylate groups which are substituted on the

terminal amine groups of the gelatin molecule. It has been widely used because it offers the flexibility of enabling thermal and photocrosslinking along with a tunable mechanical property and biocompatibility [72][76]. GelMA can act as a biomimetic hydrogel which can be crosslinked with light at different spectrums depending on the type of initiator used in the reaction[76]. For an instance, it can be crosslinked with UV light (365nm) in presence of Irgacure 2959, blue light (405nm) in presence of VA-086, and visible light (520nm) in presence of Eosin Y. Along with the ease of extrusion due to manageable viscosity and crosslinkability with various photoinitiators it has been widely used in all types bioprinting systems. Compared to pristine gelatin, GelMA exhibits an enhanced mechanical property and biocompatibility with a higher rate of cell survival and attachment.

Applications of GelMA is perhaps the most widely seen across the biofabrication arena. Recently, Spencer *et al*. utilized an extrusion-based system to print a composite hydrogel with GelMA and poly(3,4-ethylenedioxythiophene):poly(styrenesulfonate) (PEDOT:PSS)[77]. The resulting scaffold from the composite resulted in a mechanically stable, biocompatible, and electrically conductive environment which can be also be tweaked as needed. The study utilized the material properties of PEDOT:PSS and GelMA and used both chemical and visible light crosslinking and also reported high cell viability count and cell proliferation. Gelatin methacryloyl has also been used in combination with synthetic polymers like polyethylene glycol diacrylate (PEGDA) [78]. Want *et al.* used the hydrogel mix and laser-based bioprinting system to print scaffolds with enhanced printability, biocompatibility, and mechanical property under visible light. Gauvin *et al*. also reported printing porous scaffold with GelMA and HUVECs using a laser-based bioprinting system [79]. GelMA has also seen applications in droplet-based, multi-nozzle, and hybrid bioprinting systems. In 2018, Yoon *et al*. reported the approach of using piezoelectric

inkjet printing and spray-coating to form 3D free form scaffolds [39]. The study incorporated alginate with GelMA as a base component to achieve high cell viability and metabolic functionality of human fibroblasts. In a more recently published study, GelMA was inkjet printed on a stretchable substrate along with encapsulated fibroblasts which were then exposed to cyclic mechanical stress to observe the mechano-response of the cells [80]. GelMA printed at different concentrations has been reported to have variance in mechanical property, however, across all variants, cell viability was high along with sufficient cell attachment, proliferation, and consequent response to cyclic stress. The use of GelMA has also been in bottom-up biofabrication techniques. Xie *et al*. used low concentration pure GelMA microdroplets in an electro-assisted printing system [81]. The study reported the printing of low concentration pure GelMA microdroplets at a high speed and minimal cell damage. Results were able to prove the viability with the use of bone marrow stem cells within the microdroplets and predict its usage in developing organoids and drug delivery.

Alginate: A polysaccharide, often extracted from brown algae, Alginate is a naturally derived hydrogel which is well known for bioprinting applications. Alginate consists of α-L-guluronic acid (G) and β-D-mannuronic acid (M) in the molecule and crosslinks with chemical reactions with influence from ions [82]. The popularity of alginate as a candidate for 3D bioprinting application is by virtue of its biocompatibility, low cost, and ability to crosslink under various conditions including chemical reactions and photocrosslinking. Calcium Chloride ($CaCl_{2)}$ and Calcium Sulphate ($CaSO_4$) are mostly used for ionic agents for cross-linking alginate because the divalent calcium ions form a bridge due to the attraction of negatively charged carboxylic acid groups between two neighboring alginate chains [83][84]. The use of alginate has been diverse but often focus has been on encapsulating cells including stem cells, chondrocytes, and myoblasts in

a biomimetic condition where it is favorable for the cells to functions due to the mechanical integrity of the hydrogel matrix [85]. However, it is also well documented that cell attachment and proliferation within the alginate hydrogel is not possible because of the largely hydrophilic nature of the alginate molecules [86]. As a result, there is a lack of protein moieties which can facilitate cell attachment. But in order to achieve cell attachment, chemical modification of the alginate molecules with RGD groups is a viable option for enabling cell attachment in the hydrogel [87]. Extrusion-based printing systems are the most widely used systems for alginate specifically because with the use of co-axial nozzles and ionic baths one could easily crosslink alginate during printing therefore providing a much easier option. Nonetheless, the application of extrusion-based bioprinting with alginate has been diverse depending on the extrusion of the hydrogel either as a prepolymer or pre-crosslinked hydrogel. A study in 2015 used the properties of nanofibrillated cellulose along with alginate for 3D bioprinting. The printed shapes resembled that of an anatomically similar human ear and sheep meniscus which was fed to the printing system from Magnetic Resonance Imaging (MRI) and computed tomography (CT) scan data. Eventually, human chondrocytes encapsulated within the hybrid hydrogel showed high cell viability of around 86% after a week [88]. Also, because it is possible to produce droplets with alginate depending upon the concentration, droplet-based printing is feasible with alginate [89]. Moreover, laser-based printing systems have also been used with alginate in varying concentrations with different mechanical properties including matrix- assisted pulsed laser evaporation-direct write (MAPLE-DW) [90][91]. Overall the success of bioprinting scaffolds with varying technics with alginate depends on the concentration, rheology, crosslinking time, scaffold size, wettability, and ability to crosslink under laser or light [90].

Collagen: Collagen is a very popular and much sought after in bioprinting applications. This natural triple helical protein is among the major components found in connective tissues of mammals [92]. Compared to other materials used in bioprinting, collagen is often the most desirable option because not only it enhances cell attachment and growth but it also has a low immunological reaction. The abundant integrin-binding sites on collagen are responsible for the high cell attachment and proliferation within the hydrogel matrix. Despite having a numerous biological reason for using collagen, there are some material properties of collagen which are discouraged for bioprinting applications. Collagen is known to be a liquid at lower temperatures and crosslinks at higher temperatures requiring a long time. For an instance, it requires almost 30 minutes for collagen to gel at 37°C [84]. Hence, the printing time is very long but most importantly it hampers the distribution of cells within the scaffold. The longer gelation time coupled with the gravitational attraction on the cells causes them to agglomerate near the bottom surface hence hampering the homogenous distribution of cells. Moreover, collagen scaffolds are not widely known for their mechanical properties.

Extrusion-based printing has been used by Moncal *et al*. to bioprint a blend of collagen type-I and Pluronic® F-127[93]. Their system was developed to be a thermally controlled system that had optimized profiles of the bioink blend for printability and rheology. The study showed good cell viability and proliferation of rat bone marrow-derived stem cells (rBMSCs) along with collagen fiber alignment. Although, the use of collagen-based bioink in droplet-based printing systems is very limited due to its fibrous nature, however, there have been some applications. Deitch *et al*. ensured an application of inkjet printing with collagen by making sure that collagen is being deposited before crosslinking of the scaffolds. As opposed to droplet-based systems, laser-

based systems have been successful with the printing of collagen-based bioinks. Thin collagen layers that are laser-absorbing were printed by Michael *et al.* in 2013 [94].

Agarose: Agarose is a brittle natural polysaccharide that can retain its form. As a result, this hydrogel has been in use as a bioink for 3D bioprinting scaffolds. Agarose is known to gel at low temperatures and is reversible to a liquid form in the range of 20° - 70°C. Agarose, although used for bioprinting application, is not the most desirable hydrogel for hosting living cells. It is because of its limited rate of cell proliferation and activity within the hydrogel [95]. Similar to Alginate, it has poor cell attachment within the hydrogel hence oftentimes, it is seen to serve as a support material or mold [96]. However, the complications with poor cell attachment and proliferation in Agarose can be improved by using it with hydrogels that are more cell-friendly like gelatin, collagen, etc.

In 2014, Campos *et al*. used an extrusion-based system to print scaffolds of better shape fidelity with only agarose compared to a hybrid bioink with collagen and agarose. The study reported that although the printing fidelity was found to be very good, the cells within the hydrogel remain viable and confined in circular shape without much evidence of proliferation [97]. Agarose has also been deployed in the droplet-based printing systems with the use of micro-valves and has been known to achieve a high number of live cells within the structure [98]. Nonetheless, the high viscosity of agarose is an inconvenience for droplet-based bioprinting because it leads to clogging of the nozzle. Lastly, a study by Koch *et al*. shows that Agarose can be a very good fit for laser-based bioprinting by virtue of its viscosity and is also able to retain a high count for live cells within the matrix [99].

1.2.2 Synthetic Bioinks

In addition to the use of natural polymers as materials for bioinks, there have also been applications of synthetic materials in bioink development. Like natural hydrogel, synthetic hydrogels offer different specific advantages that make their use convenient for 3D bioprinting applications. Hosting cells within the matrix of a synthetic hydrogel is also possible and widely research. Natural hydrogels offer environments that are more similar to native environments for the cells, in that regard synthetic hydrogels can provide environments that are more predictable for researchers, stable, and easily tunable for application depending on the requirements.

Oftentimes, synthetic hydrogels are preferred over natural hydrogels because they tend not to interfere with the immune system of the biological units. That is why utilizing synthetic hydrogels can help avoid immunological reactions within the hydrogel and upon implantation. Moreover, since synthetic hydrogels can be produced in a controlled environment, therefore, the batch to batch variance and unexpected outcomes from reaction or purification remnants can be avoided[100]. In addition to these, using synthetic hydrogels allows for the fabrication of scaffolds that are easily tunable to desired mechanical, chemical, and transport properties. Overall, it evident that synthetic hydrogel can also provide a wide scope of applications in 3D bioprinting specifically due to their batch-to-batch consistency, modifiable properties, ease of production, and non-immune responsiveness.

Pluronic F-127: Pluronic F-127® is a commercially available synthetic polymer poloxamer-based compound. There are 11 different types of Pluronic® polymers which can be differentiated based on their functionality, crosslinking temperature, molar mass, and composition. Typically, Pluronic can crosslink with increased temperature in the range of 10-40°Cwhere two hydrophilic blocks are found in between hydrophobic blocks and it can also undergo reverse gelation [101]. It is biocompatible to the extent that it can host cells within its matrix for up to 5 days without any

required modifications or additives. Although, typically the copolymer structure of Pluronic is not the best example for structural integrity. However, when combined with other polymers—it performs well in a variety of applications. For instance, Gonge *et al*. combined Pluronic with polyethylene glycol (PEG) for controlled release and drug delivery usage [102]. In addition to initiating crosslinking in Pluronic® thermally, it can also be photocrosslinked with UV depending upon the usage of specific photoinitiators. The duration of UV used on the polymer and the concentration of the photoinitiators are known to affect cell viability as well[103]. Furthermore, its mechanical properties can also be enhanced using chemical crosslinking methods. By virtue of its gelation behavior, it requires a nozzle heating system and a heated printer platform with extrusion-based systems. The heating system ensures that there is no clogging in the nozzle and good structural integrity of the scaffolds post-printing. Due to the temperature sensitivity, it is troublesome to handle Pluronic® because it requires the use of a temperature controlling apparatus which makes the printing expensive. Therefore, due to the difficult rheology profile and thermo-responsiveness of Pluronic®, it has not been very popular with laser-based or droplet-based applications as well.

Poly(ethylene glycol): A hydrophilic polyether, Polyethylene glycol (PEG) is one of the most popular choices as a synthetic material for bioprinting. A water-soluble synthetic polymer that can be conjugated with various biomolecules is a desirable candidate as a bioink[84]. Modification of PEG can also allow for enhancement in mechanical properties and photocrosslinking in the presence of photoinitiators. Pristine PEG does not exhibit very good mechanical properties for scaffold printing. That is why, oftentimes, the PEG molecule is modified with diacrylate (DA) or methacrylate (MA) groups which allow for crosslinking under different spectrums of light including UV and laser.

The use of modified PEG—namely PED-DA & PEGDMA is widely evident in all bioprinting systems. Extrusion based systems utilizing this synthetic hydrogel as a scaffold are numerous where printability and mechanical structure integrity has been focus [104] [105] [106]. Moreover, as a consequence of better mechanical properties like higher compressive modulus—modified PEG has been widely used in droplet-based systems[107]. Laser-based systems also saw the use of modified PEG because of photocrosslinkability. For instance, Cui *et al*. reported the bioprinting of the osteochondral plugs with a layer-by-layer laser-based printing system utilizing a UV illumination source [108][107]. Hribar *et. al* also utilized a laser-based system[61]. SLA bioprinting techniques under laser-based systems are also very popular because of the ease of processing with modified PEG. Wang *et. al* used an SLA-based system with a hybrid bioink of GelMA and PEGDA to print and produce highly viable 3D printed scaffolds[65]. Dhariwala *et. al* reported a 90% cell viability of Chinese hamster ovary cells with the use of PEGDMA[109].

1.3 Research Objectives

Considering the current bioprinting strategies and limitations of available bioinks, it is important to identify and develop bioinks that can mimic native tissue conditions more accurately. There is a surge in the utilization of biomaterials that are native to the human body for tissue engineering applications. Due to the abundance of hyaluronic acid in the extracellular matrix of brain and cardiac tissues, the development of a hybrid photocrosslinkable hyaluronic acid-based bioink is desirable for cardiac and neural tissue engineering. The goal of this research has been divided into the following objectives:

Objective 1. Synthesis of a photocrosslinkable hyaluronic acid-based hydrogel: The synthesis of photocrosslinkable bioinks is widely seen through the substitution of the methacrylate group on polymer molecules. However, the substitution of methacrylate groups on hyaluronic acid molecules poses a significant challenge. Therefore, a protocol for the reliable synthesis of methacrylated hyaluronic acid-based hydrogel (MeHA) with a high degree of substitution will be developed.

Objective 2. Development of GelMA-MeHA-based cell attachable hybrid bioink: Tissue engineering and bioprinting applications require the hydrogel to facilitate the growth and proliferation of cells within the scaffold. Therefore, it is essential for a bioink to be bioactive and provide a suitable substrate for the cells to adhere. A hybrid bioink will be developed and characterized by combining MeHA and GelMA as complementary constituents.

Objective 3. Characterization and stereolithography based bioprinting of GelMA-MeHA hybrid bioink: The hybrid bioink developed in previous objectives will be further utilized in bioprinting by a DLP-SLA system to establish its applicability in fabricating tissue analogues.

Considering the aforementioned objectives, this thesis has been organized in the following manner to provide a comprehensive view of the development of the GelMA-MeHA hybrid bioink:

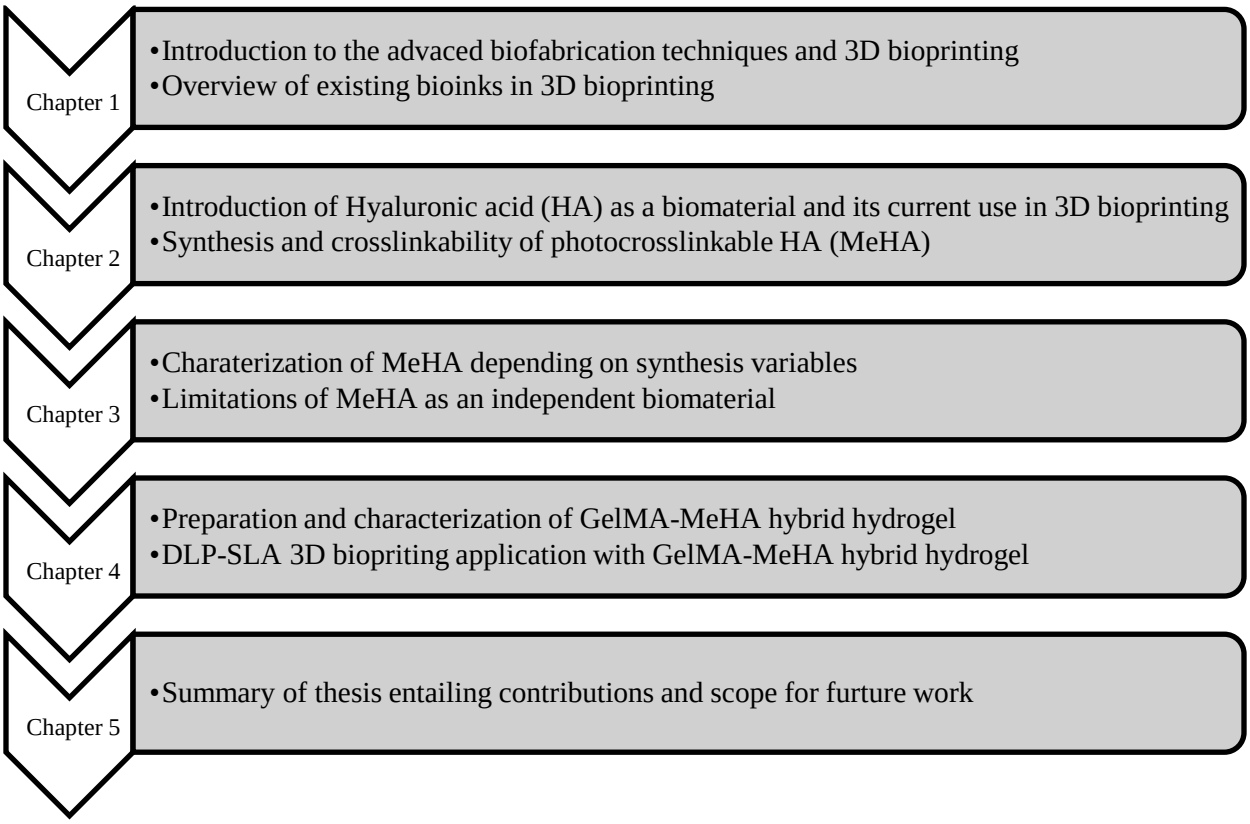

Chapter 2: Dual-crosslinkable HA-based Bioink

Chapter 2 dives into the discussion about hyaluronic acid as a biomaterial and evaluates the existing application of this biomaterial in diverse bio-fabrication applications. As the ground is set, a synthesis protocol for the development of photo-crosslinkable hyaluronic acid-based bioink is proposed, which is then validated through photo and thermal crosslinking.

2.1 Hyaluronic Acid

Hyaluronic acid (HA) is a naturally existing polysaccharide that consists of disaccharide repeating units of D-glucuronic acid and N-acetyl-D-glucosamine and has β (1-4) linked 2-acetamide-2-deoxy-D-glucose and β (1-3) linked D-glucuronic acid [110,111]. Found primarily in synovial fluid, umbilical cord, and connective tissue of most animals, HA has also been found in the streptococci group [112]. After its discovery, it has been used for diverse applications due to its anti-inflammatory response, disinfecting, and wound rehabilitating capabilities. It is known to enhance the healing of epithelial cells, helps reduce swelling, scars, and also protects tissues in the vitreous humor [112].

The molecular weight of the HA available for use is typically between 120 –2500 kDa due to which its properties are known to vary. It has been reported that whereas high molecular weight HA restricts the inflammatory responses in macrophages which results in phenotypic changes, the opposite is true for low molecular weight [113]. Furthermore, *in-vitro* studies have shown that gels resulting from the different molecular weight of HA increases cell proliferation and reduces inflammation in synovial joints [114]. From a bird's eye view, HA seems to have the following advantages [115]: (a) It is a biocompatible and biodegradable material. (b) It is found in the human body as an intracellular component that aids lubrication, differentiation, and growth of cells. (c)

HA molecule is involved actively in the wound healing process, as a result, it can accelerate the wound healing in bioprinted scaffolds. (d) Its specific and non-specific protein absorption and interaction with cells enable the possibility to use it with CD44, RHAMM, ICAM-1 receptors.

Therefore, due to evidence suggesting a wide range of biologically important properties – the role of HA in biofabrication techniques has been widely investigated in recent years. The key approach to incorporate HA with advanced biofabrication techniques and additive manufacturing has been around the development of hyaluronic acid-based bioink. When it comes to additive manufacturing-based applications, extrusion-based 3D bioprinting, among other methods, is prominent due to the ease of technology comprehension. That is why the initial attempts with HA have been with extrusion bioprinting systems. However, there is a research gap in the use of HA for other bioprinting modalities. Hence, there is room for further work in this area. Besides using HA as a sole bioink, HA has seen applications where it has been used as a component of a hybrid bioink and also as a stand-alone additive material. Considering these, the investigations into the use of HA in 3D bioprinting can be divided into the following approaches branched into:

1. Hyaluronic acid as an independent bioink
2. Hyaluronic acid as a component of a hybrid bioink
3. Hyaluronic acid as an additive component in bioink

2.1.1 HA as an Independent Bioink

The use of hyaluronic acid in biofabrication techniques as an independent material is seldom seen. In 2015, Kesti *et al*. reported an HA-based versatile bioink that enabled photocrosslinking and thermoresponsiveness through the use of poly(N-isopropylacrylamide) (pNIPAAM) grafted on the HA molecule. The group integrated PNIPAAM with HA to address the lack of structural

fidelity with only methacrylated HA and achieved quick crosslinking and long-term mechanical stability of the printed structures. Furthermore, they reported good cell viability with chondrocytes once the pNIPAAM was removed from the scaffold post-printing. On the other hand, Burdick and his group reported the development of a bioink that works on the guest-host principle depending on the presence of shear-thinning for force [116]. They further investigated the hydrogel for its rheological property, degradation, and effect *In vivo*. An application of only methacrylated HA (MeHA) for bioprinting is seen in the work by Poldervaart *et al*. where they utilized 3% MeHA to bioprint constructs and tested its biocompatibility with mesenchymal stromal cells [117]. They report cell viability of around 60% after 21 days and mention that the stem cells were able to go through osteogenic differentiation. The approach utilized UV light for crosslinking the hydrogel scaffolds and the rheological, physical, and visco-elastic properties of the developed MeHA were also characterized.

As evident from the discussion above, the use of HA as an independent material for biofabrication strategies-especially for bioprinting techniques is not widespread because of the challenges it poses. The poor rate of substitution of methacrylate groups on the HA molecules makes photocrosslinking a difficult avenue. Moreover, the rheology profile, poor mechanical properties, and the lack of cell-attachment within the pristine HA scaffold are concerns that need to be addressed for it to be viable as an independent bioink.

2.1.2 HA as a Hybrid Bioink

Often, HA is used in a blend with other natural or synthetic biomaterials [111]. The use of protein conjugates is a popular option as it enables cell attachment within the hydrogel matrix. Moreover, the use of additional polymer or biomaterial can help address the issues with poor

mechanical properties and photocrosslinking. Gelatin methacryloyl (GelMA) being a popular and a standalone viable bioink, researchers have often resorted to its use with MeHA [118–123]. Skardal *et al*. developed methacrylated HA with a degree of substitution of only 5% and used it with GelMA hydrogel for a two-step bioprinting process[121]. The group printed core-shell structures and utilized multi-step crosslinking methods to ensure proper crosslinking with UV lights. The study confirmed biocompatibility with the 3T3 fibroblast cells. O'Connell *et al* developed a Biopen which utilizes a GelMA-MeHA hybrid hydrogel for printing [123]. The group proposed the use of a biopen for freeform bioprinting during surgery and proves the biocompatibility of the bioink through the use of human adipose stem cells. However, most of these studies report MeHA with a very poor degree of substitution (DS) and often use HA in a very small concentration. Without a specific application in consideration, all of these studies report the crosslinking of MeHA with UV light only. Furthermore, the use of MeHA has also been noticed with other popular biomaterials like Alginate, Collagen, Cellulose etc. [118,124–126]. Using MeHA with complementary biomaterials makes it convenient for researchers to overcome some of the shortcomings that this material poses. As a result, combining it with other substances has been a popular approach that yielded results that show promise for its use in bioprinting.

2.1.3 HA as an Additive

Besides the aforementioned approaches, the HA has also seen its use as an additive in other hydrogels to improve physical properties like visco-elasticity, mechanical strength, and biocompatibility. Synthetic polymers offer very little in terms of biocompatibility when they are used in bioprinting applications. Therefore, biocompatible materials like HA is often introduced so that the encapsulated cells thrive within the scaffold. In addition, the application of HA as an

additive is usually due to its visco-elastic property and its contribution to enhancing the mechano-physical property [127–130]. For an instance, Müller *et al* used synthetic polymer pluronic F127 along with MeHA with DS of only 0.7% to introduce a biophysical cue within the scaffold and also increase the mechanical stability of the scaffolds [127]. In another study by Skardal *et al*., modified HA was used with thiolated gelatin to act as a visco-elastic agent [128].

The viscosity and mechanical strength offered by HA has long been utilized in the surgical and cosmetic industry. Therefore, it must also offer new avenues for researchers involved in developing biofabrication techniques.

2.2 Challenges in Methacrylation of HA

The use of hyaluronic acid as a bioink involves modifying the polysaccharide in some manner so that it is compatible with existing additive manufacturing processes. Like many other hydrogel materials used in 3D bioprinting, methacrylation of the hyaluronic acid molecule to enable photocrosslinking is among the existing approaches. The development of methacrylated hyaluronic acid (MeHA) has paved the way for using HA as a bioink to produce stable cell-laden scaffolds using the existing 3D bioprinting methods.

However, compared to the common biomaterials, there is a significant challenge when it comes to modifying the hyaluronic acid to enable photocrosslinking. Photocrosslinking is often the primary method for post-printing crosslinking because unlike alginate, enzymatic, or ionic crosslinking with hyaluronic acid is not feasible. Moreover, photocrosslinking offers freedom and a wide range of options in terms of printing techniques.

Utilizing methacrylic anhydride as a methacrylating agent with 2% hyaluronic acid, Kimberly *et al*. were among the pioneers to develop a stable and characterizable hydrogel with a

well-defined and reproducible protocol [110]. The protocol involved the reaction of the reagents at 5°C for 24hrs which resulted in a 14% DS on the carbohydrate molecule. It is important to understand that the DS is a key factor that dictates photocrosslinking. The greater the DS the easier it is to crosslink the polymer using a radical generating initiator. It not only defines, how fast the crosslinking can take place but also affects the crosslinking density and consequently the mechanical property. When compared, DS reported for MeHA is very low relative to popular bioinks like GelMA which go up to 90% and above. As a result, there have been efforts to increase DS in MeHA to enable better and easier photocrosslinking with MeHA for 3D bioprinting applications.

For instance, a DS of 5-7% was reported by Poldervaart *et al*. which dissolved HA overnight in a 3:2 ratio of reverse osmosis (RO) water and dimethylformamide (DMF) for better dissolution followed by the addition of 1.5-3x molar equivalent methacrylic anhydride (MA) while maintaining the pH between 8-9. The synthesis was carried out for 16 hours at 4°C [117]. The synthesis was performed in similar conditions by Khademhosseini's group and a 20% DS was reported which only used DI water with 1% MA for 24 hours at 4°C [122]. Furthermore, Leach *et al*. carried out their synthesis at room temperature followed by incubation at 60°C for 1 hour. Their process involved using Glycidyl Methacrylate (GMA) with Triethylamine (TEA) and Tetrabutylammonium bromide which was reported to show a DS of 11% [131]. Hatchet *et al*. reported a DS of 10-50% with a 3:2 mixing ratio of DMF and ultra-pure water as the solvent. The methacrylating agent used in this study was methacrylic anhydride and the reaction was carried out at 4°C for 16 hours.

The mentioned studies and their reported DS with HA show that there is a lack of clear and stable protocol that can attain the desired level of DS. When utilized in bulk manufacturing

processes like 3D bioprinting, the development of such a reliable protocol is required. Therefore, it highlights the challenge that researchers in this area are facing with the methacrylation of HA.

2.3 Synthesis of MeHA

The synthesis of photopolymerizable MethacrylatedHyaluronic acid (MeHA) hydrogel was done with modification to the protocol reported by Bencherif *et al* in 2008 [132]. Briefly, 1g of Hyaluronic acid (HA) sodium salt from Streptococcus equi (Sigma-Aldrich) was measured. In order to facilitate the dissolution of HA salt, a solvent with a 2:1 ratio of 200 mL phosphate buffer saline (PBS) and 100 mL dimethylformamide (DMF) was prepared. DMF was added to the PBS slowly to ensure that there is no phase separation between the two liquids. The solvent was stirred for 30 minutes at 4°C, the temperature at which the whole synthesis process was carried out. Afterward, the HA salt was slowly added to the solvent to ensure that no lumps were formed. The HA salt is left overnight to completely dissolve with continuous stirring at 4°C. After complete dissolution, the methacrylating agent Glycidyl Methacrylate (GM) was added dropwise (28.462 mL) to the solution in 100-fold molar excess along with 7.26 mL of triethylamine (TEA). The reagents were left to react at 4°C with continuous stirring for varied time frames – 3 days, 5 days, and 10 days – to obtain 3 different types of MeHA based on the degree of substitution. Once the reaction was complete, the solution was transferred to dialysis tubing (12-14 kDa) (Fisher Scientific, Waltham, MA, USA) and dialyzed against RO water for 3 days. The water was changed twice every day until completion. The filtered solution was then frozen at -20°C and then lyophilized to obtain cotton-candy like solid MeHA.

Figure 2.1 (B) illustrates the reaction mechanism that takes place to produce MeHA in presence of Glycidyl Methacrylate (GM) and Triethylamine (TEA) which is present as a catalyst.

As the reaction proceeds, there are two reaction pathways a) reversible transesterification and b) ring-opening conjugation are known to take place simultaneously resulting in the substitution of methacrylate groups on the hyaluronic acid molecules [133]. Reaction pathway a, the reversible transesterification reaction, is only able to substitute the hydroxyl groups on the hyaluronic acid chain temporarily. The reversible nature of the reaction results in a low permanent substitution yield. However, reaction pathway b is irreversible in nature and only takes place through the ring-opening conjugation at the carboxylic acid group site and results in the greatest amount of permanent substitution compared to a. Therefore, in order to facilitate high DS, reaction pathway b should be favored. Initially, the rate of reversible transesterification is high which begins to diminish with time and subsequently reaction b picks up resulting in epoxide ring-opening conjugation. Since epoxide ring-opening reactions only begin to play a major role after 5 days hence reactions with less than 5-day duration would yield a very low DS [132]. Additionally, favorable reaction conditions and solvents can play an important role in the synthesis. Bencherif *et al*. reported that low temperature facilitates a high DS due to its effects on the hydrolysis of GM [132]. The group carried out the reaction at 50°C and 25°C and reported that the lower temperature had a positive effect in enhancing DS. Considering this and other studies, the synthesis was run at 4°C which is further lower than 25°C expecting to create more optimum reaction conditions for enhancing DS. Also, the use of DMF as a co-solvent helped to increase the solubility of the HA sodium salt and GM in the reaction mixture, therefore, ensuring higher reaction efficiency.

Besides the synthesis, post-synthesis filtration and processing should be chosen carefully considering effectiveness and cost. Therefore, instead of precipitation, a dialysis process was followed. Rather than the use of large volumes of ethanol or acetone for precipitation, the use of RO water for dialysis is just as effective in removing toxic remnants.

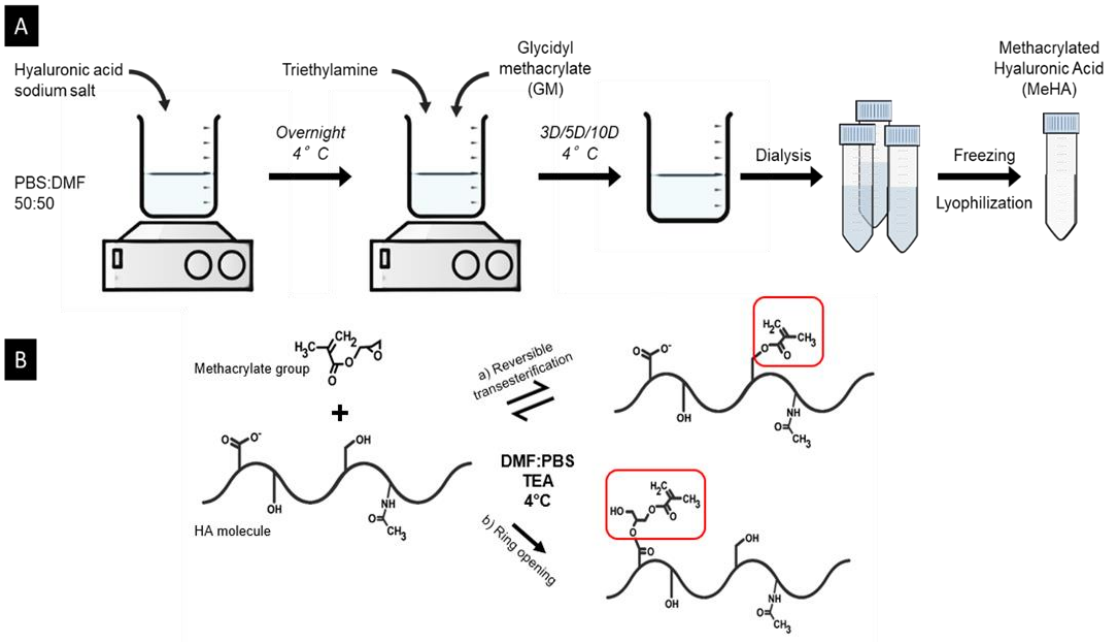

Figure 2.4. Methacrylation of Hyaluronic acid (HA) (A) Schematic of a synthesis protocol for the methacrylation of Hyaluronic acid (HA). (B) Substitution of the methacrylate group takes place by a) Ring-opening or b) Reversible transesterification.

The developed protocol utilizes the best practices from all the reported studies reviewed[110,132]. Therefore, it can maximize the utility and result in the highest possible DS. Moreover, to evaluate the effect of reaction duration on the DS and subsequent properties of MeHA, three different syntheses were carried with three different synthesis duration (3-day, 5-day, and 10-day). The synthesis product was denoted by their reaction time, namely 3-day MeHA, 5-day MeHA, and 10-day MeHA. Depending on the duration of the synthesis, the physical, rheological, and crosslinking properties of MeHA may change and these variants offer the opportunity to understand these differences in the property. After the synthesis, the physical appearance of the lyophilized hydrogel and viscosity was also examined. Through these observations, it was observed that the length of the synthesis had an impact on the appearance of

the lyophilized hydrogel, dissolution time, and resultant viscosity. Among the three types of MeHA, 10-day MeHA produced the very light and cotton-candy-like lyophilized hydrogel. It seemed to be the least dense among the three which had the quickest dissolution time in RO water and PBS resulting in the least viscous solution. As the reaction time decreased, the corresponding MeHA seemed denser which took longer to completely dissolve and produced more viscous solutions. A possible explanation, among many other physical reasons, that led to the reduction of viscosity is the likely gradual breakdown of the long HA polymer chains with time. Therefore, as the synthesis duration is increased, shorter polymer chains are obtained due to their gradual breakdown which results in less viscous solutions.

These physical features of the three types of MeHA developed could have major consequences in determining their usage. For example, less viscous 10-day MeHA can be more useful for applications where more hands-on manipulation and dispensing are involved hence enabling easy transfer of the hydrogel solution with the least shear stress. On the other hand, 3-day MeHA producing more viscous solutions might be relevant in an application where viscosity enhancement material or friction-reducing material is required. Hence, the attempt to perform the reaction at three different durations not only results in a clearer understanding of DS on HA molecules but also led to the development of three different products that can have diverse applications.

2.4 Crosslinking Mechanisms for MeHA

The primary goal of substitution of methacrylate groups on the HA molecule is to enable the capabilities of photocrosslinking so that HA becomes compatible with the current additive

manufacturing-based biofabrication techniques. Therefore, post-synthesis, the crosslinkability of the developed MeHA was assessed.

2.4.1 Photocrosslinking

The photoinitiator used for the crosslinking of methacrylated hyaluronic acid (MeHA) was an EY-based photoinitiator. The base concentration of the reagents were 2 mM eosin Y disodium salt (Sigma-Aldrich) and 20% w/v triethanolamine (TEOA) (Sigma-Aldrich). 100x concentrated stock solutions of 2mM EY (0.01384 g/10mL) and 20% w/v TEOA (20g/100mL) were prepared with phosphate-buffered saline (PBS). The final composition of the bioink comprised of 0.02 mM eosin Y and 0.2% w/v TEOA.

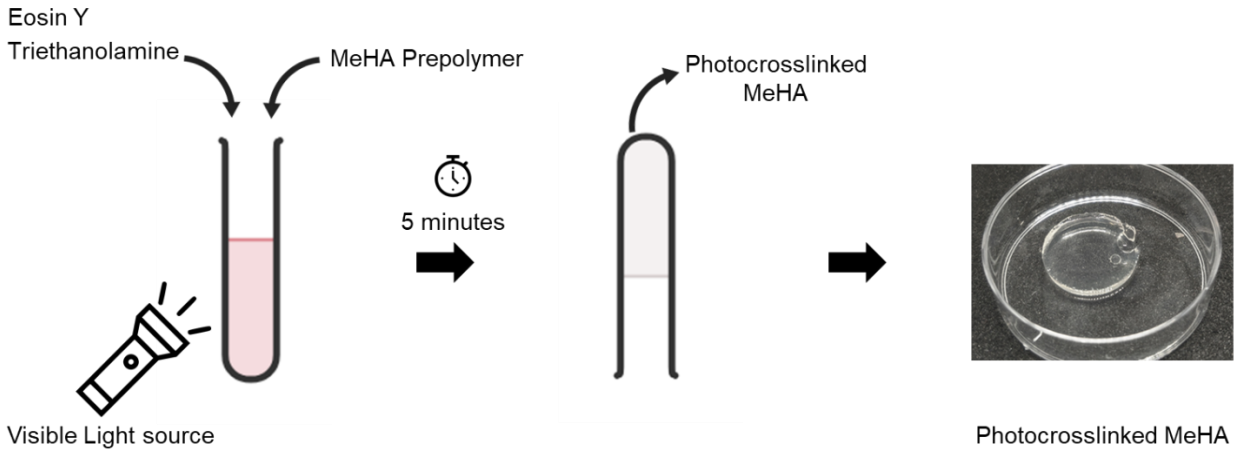

Figure 2.5. Visible light crosslinking of Methacrylated Hyaluronic acid (MeHA) using EY based photoinitiator

Typically, for 1 mL solution of hydrogel precursor, 10 µl of 100x TEOA and 20 µl of 100x EY were used. After the preparation of the polymer precursor with the photoinitiator, the precursor mixture was dispensed into a 24-well plate and exposed to visible light in the DLP-SLA bioprinter.

Consequently, the polymer precursor completely crosslinked in the shape of a disk after 5 minutes of exposure to visible light. The crosslinking time for MeHA is dependant on the DS of the MeHA used. Therefore, 10-day MeHA crosslinked fastest (5-minutes), followed by 5-day MeHA (6-minutes), and finally, 3-day MeHA (8-minutes) would take the longest due to the least DS on the HA molecule. The most visible difference between MeHA and other existing crosslinked biomaterials is that MeHA produces completely clear and optically transparent hydrogel. This property can be a key differentiator when MeHA is being compared to others because it would facilitate examination by optical microscopy and prove valuable in applications demanding optically transparent materials like corneal tissue engineering.

2.4.2 Thermal Crosslinking

The initiator used to induce thermal crosslinking of methacrylated hyaluronic acid (MeHA) was 2,2'-Azobis[2-(2-imidazolin-2-yl)propane]dihydrochloride, more commonly known as VA-044 (FUJIFILM, Wako Pure Chemical Corporation). The base concentration of the initiator used was 100 mM of VA-044 prepared with phosphate-buffered saline (PBS). For instance, around 4 % w/v solution of MeHA was prepared with 485 µl of PBS, and 15 µl of 100 mM V-044 was added to the solution to obtain a final concentration of 30 mM of VA-044. The entire solution was vortexed for homogeneous mixing, and then it was left at 37ºC in a water bath for 30 minutes. After the incubation time, the hydrogel completely crosslinked, as shown in Figure 2.3

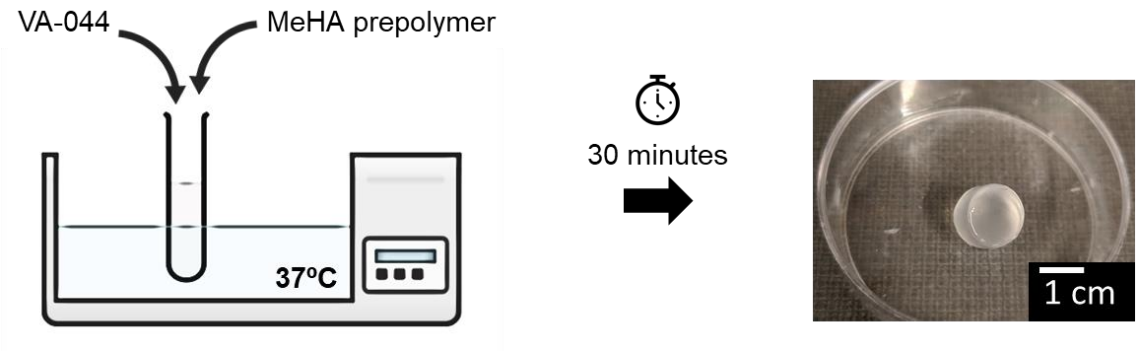

Figure 2.6. Thermal crosslinking of MeHA using VA-044

The thermal crosslinking capabilities could enhance several things and open new possibilities for MeHA. It can be utilized in a hybrid crosslinking mechanism. For an instance, if a 3D bioprinting technique like DLP-SLA is considered, then it can greatly help in crosslinking any remaining un-crosslinked remnant after printing during incubation without causing over crosslinking or change of the desired shape. Therefore, not only the mechanical strength of the printed scaffold will be enhanced but the degradation is also slowed down significantly. Moreover, as the half-life of VA-044 is not more than 10 hours, therefore, it would be removed from the scaffold within 24 hours of incubation. Since the crosslinking is able to take place at 37°C hence it also opens the possibilities of using MeHA and crosslinking them *In vivo*.

The studies conducted in the next portions of the thesis, do not utilize thermal crosslinking or implement the dual-crosslinking characteristics of MeHA. This has been conducted as a proof of concept and keeping future applications of MeHA in mind.

2. 5 Chapter Summary

In chapter 2, hyaluronic acid as a biomaterial is elucidated. A review of the literature on the existing studies using hyaluronic acid and its application in additive manufacturing-based

biofabrication techniques is performed. Afterward, the developed synthesis protocol for the development of methacrylated hyaluronic (MeHA) acid is discussed. The rationale behind the choice of reaction conditions and duration is objectively evaluated. Eventually, a difference between the three types of MeHA developed is established with preliminary observations. Finally, the developed hydrogel is tested for its crosslinkability using visible light and temperature.

Chapter 3: Characterization of MeHA Bioink

The synthesis protocol described in Chapter 2 resulting in three types of MeHA, namely 3-day MeHA, 5-day MeHA, and 10-day MeHA, are different in characteristics by virtue of their duration of synthesis and DS. Chapter 3 describes the techniques used to characterize the three types of MeHA developed. To do so, the DS, mechanical properties, and biocompatibility are evaluated. These results would help provide insights into understanding the properties of MeHA and its variants. Hence, it could shed light on how each variant of MeHA can have a requirement specific application.

3.1 Substitution of Methacrylate Group on HA Molecules

As discussed in Chapter 2, the substitution of the methacrylate group on the HA molecule is key to enabling photocrosslinking. The amount of successful substitution of methacrylate groups on the HA molecule determines the degree of substitution (DS). The most common technique to find out the DS is to examine the molecular structure of the product through NMR spectroscopy.

3.1.1 ^{1}H NMR Analysis

The DS of methacrylate groups on the hyaluronic acid molecule was examined by using H^1 NMR analysis. First, 3% prepolymer solutions of MeHA (3-day, 5-day, 10-day) were prepared using Deuterium Oxide (D_2O) and dissolved overnight to ensure complete dissolution. The prepolymer solutions were then transferred into NMR tubes and tested with Varian MercuryPlus 400 MHz NMR spectrometer (Varian, Inc., Palo Alto, CA, USA). All tests were run at normal room temperature and pressure, at a 15Hz sample spinning, 1s relaxation delay, 45° tip angle, and for 64 scans. Finally, the NMR spectra obtained were analyzed to find the number of methacryloyl

groups per HA repeating unit. The methacryloyl peaks located at 6.1 ppm, 5.6 ppm, and 1.85 ppm were compared through relative peak integration with 1.9 ppm HA's methyl proton peak [132]. The DS is calculated from the ratio of the relative peak integration of the HA's methyl proton with the methyl proton.

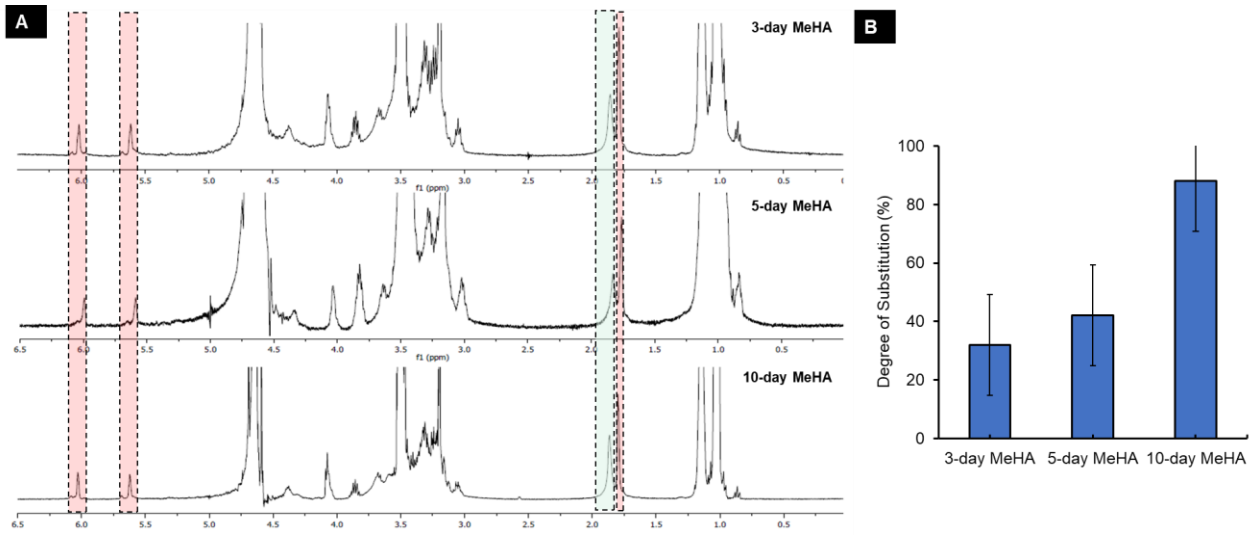

Figure 3.7. (A) NMR spectra for synthesized 3-day MeHA, 5-day MeHA, and 10-day MeHA.(B) Quantitative representation of DS obtained from the samples

The NMR spectra retrieved from the scans were analyzed and the data was used to calculate the DS. As discussed earlier, it is known that the epoxide ring-opening reaction pathway results in the permanent substitution of methacrylate groups on the HA molecule. Since reaction pathway b (See Figure 2.1 (B)) only starts to pick up after day 5 hence it can be expected that 3-day and 5-day MeHA would have low DS compared to 10-day MeHA. However, it would also be beneficial to understand if the use of DMF as a co-solvent and 4ºC temperature can enhance the DS before day 6. After analysis of the NMR spectra obtained, this hypothesis was confirmed and enhanced DS was observed for all the synthesis. The relative integration of the HA methyl proton peak at

1.9ppm, when compared to methacryloyl peaks at 6.1 ppm, 5.6 ppm and 1.85 ppm, gave a DS of 32%, 42%, and 88% for 3-day MeHA, 5-day MeHA, and 10-day MeHA. These results show that the duration of the synthesis had a clear effect on the DS.

Table 3.1. Previously reported DS on MeHA

Reaction conditions	**Degree of Substitution**	**Reference**
24 hours on ice	7%	[134]
24 hours at RTP	11%	[131]
24 hours at 4°C	20%	[122]
48 hours at 50°C	30%	[135]

Table 3.1 shows some of the studies which also report the methacrylation of hyaluronic acid. It highlights some of the reaction conditions for synthesis and their corresponding DS. Considering these reported data, a clear difference is established between the developed protocol and the previously reported studies. The minimum DS of 32% acquired with 3-day MeHA is greater than any of the reported DS in Table 3.1. The 2% difference in DS with 3-day MeHA compared to the 30% DS reported through a 2-day in Table 3.1 shows that there is a very small scope of enhancement before day 5 which validates the reaction mechanism. Subsequently, the 5-day MeHA shows a 31.25% increase in DS when compared to 3-day MeHA. It shows that post day 3 and even at day 5 major improvement awaits. Finally, the DS of 88% in 10-day MeHA is an incredible enhancement on the DS compared to the other two types of MeHA developed and the previously reported studies. It is among the highest reported DS achieved with MeHA. Therefore, the NMR analysis is able to make a clear distinction between the three types of MeHA developed based on their DS. Moreover, by looking at the DS and the corresponding reaction length, clear

conjunction between the length of synthesis and DS is established and the explanation of the reaction mechanism is validated.

This correlation between the duration of synthesis and the DS is not only a validation of the reaction mechanism but it is also an indication that this protocol is tunable per requirement. Meaning, based on the need for DS, optimum reaction time can be selected. If a high DS is not required for a specific application then it would be unnecessary to run the synthesis for a long time. However, since the rheological property is also linked to the length of synthesis, as discussed in Chapter 2.3, there would be a trade-off between the DS and viscosity. It would be unlikely to have a MeHA with high viscosity and high DS as things stand. Thereby, these finding would provide researchers an opportunity to opt for an optimum length and rheological property as deemed fit.

3.2 Mechanical Strength

The mechanical properties of the hydrogels were assessed by measuring the compressive modulus of the crosslinked hydrogels which reflects the mechanical stiffness through the Hertz contact mechanics model. In this type of indentation mechanical test, a probe is brought in contact with the hydrogel which performs a small indentation on the surface of the hydrogel and then retracts back. It is a local compressive test that requires a very small area and amount of material hence it is cost-effective and convenient [136].

3.2.1 Compressive Modulus

The probe used for the mechanical tests is custom made into a flat-ended rigid cylinder with an elastic half-space. In order to prepare samples, 2mL solution of the hydrogel precursor was prepared as described in Chapter 2.4.1 and transferred in a small petri-dish which resulted in a

2mm thick layer of hydrogel solution. The precursor was then crosslinked with visible light in 30 minutes due to the large volume used using the SLA bioprinting. The crosslinked hydrogel samples were then submerged in PBS for 24 hours and kept at a 37°C incubator to ensure that they were completely swollen. Afterward, a vertical axis micromechanical testing machine (Mach-1 v500c, Biomomentum Inc., Montreal, QC, Canada) along with a flat-cylindrical probe was used to measure and record the force vs displacement plots. Approximately, 10% strain was put on the hydrogel surface to obtain the plots and the linear region was selected to calculate the slope. Finally, the compressive modulus (E) was calculated using the following formula:

$$E = \frac{m \times (1 - v^2)}{2r} \qquad (1)$$

Here, E is denoted as the compressive modulus, m is the slope obtained from the force-displace plot, r is the radius of the probe and v is the Poisson's ratio (0.5 for MeHA and GelMA hydrogel).

The data collected and presented for the mechanical tests are presented as mean ± standard deviation. All further statistical analysis was performed by using MATLAB ™ (Mathworks, Natick, MA, USA). The significance comparison test was carried out here and later in the thesis was done using a one-way analysis of variance using Tukey's multiple comparison test. The resulting difference were significant at $p < 0.05$ with the significance levels as following – non significant (ns) $p > 0.05$, * $p < 0.05$, ** $p < 0.01$, *** $p < 0.001$ and **** $p < 0.0001$

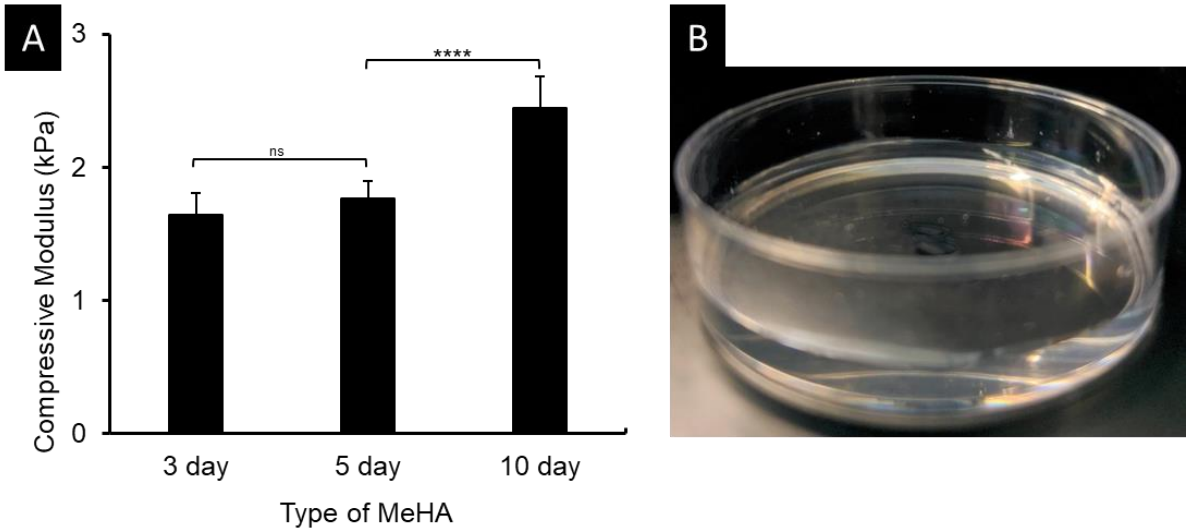

Figure 3.8. Mechanical Properties of MeHA (A) Compressive modulus of the three different types of MeHA hydrogel (B) Crosslinked 3-day MeHA hydrogel samples used for mechanical tests (n = 10; * $p < 0.05$, ** $p < 0.01$, *** $p < 0.001$ and **** $p < 0.0001$).

The DS is one of the most significant metrics when it comes to evaluating methacrylated hydrogels because it often becomes a differentiating factor. The synthesis protocol resulted in a different DS on each type of MeHA. Here, with the mechanical tests, it would be possible to discern how that plays a role in determining the mechanical stiffness of the hydrogel. DS is key to crosslinkability and thereby determines the time needed to crosslink, the crosslinking density, and consequently the mechanical property. A high DS is expected to have high mechanical stiffness with a short crosslinking time and vice versa. The compressive modulus of the three types of MeHA is able to reflect the importance and influence of DS on the mechanical property.

The data from the mechanical tests show that the 3-day MeHA has a compressive modulus of approximately 1.64 kPa which only increases to around 1.77 kPa in the 5-day MeHA. This reflects that a 10% change in DS from 3-day MeHA to 5-day MeHA is only able to increase the mechanical stiffness of the hydrogel by 8%. It shows that major changes in structural integrity and

mechanical property cannot be expected with a small change in synthesis duration. Therefore, it can also be inferred that with lower than 32% DS, the mechanical stiffness of MeHA would be extremely low hence its use with 3D bioprinting techniques will be increasingly problematic. However, the 10-day MeHA shows promise. It has exhibited a compressive modulus of 2.44 kPa which is an almost 50% increase in mechanical stiffness when compared to 3-day MeHA. This significant increase again points out to the importance of achieving a high DS. Due to the high DS, there is at least twice as much increase in the crosslinking density in 10-day MeHA hence the enhancement in the mechanical stiffness. Table 3.1 helps summarize the relationship between DS, viscosity, and mechanical property achieved in the three types of MeHA.

Table 3.2. Summary of properties of MeHA based on DS, Viscosity, and Compressive Modulus.

	High Viscosity	**Moderate Viscosity**	**Low Viscosity**	
High DS	-	-	10-day MeHA	High Compressive Modulus
Moderate DS	-	5-day MeHA	-	Moderate Compressive Modulus
Low DS	3-day MeHA	-	-	Low Compressive Modulus

3.3 Biocompatibility

The MeHA hydrogel developed through the proposed protocol was intended to be used for tissue engineering and 3D bioprinting. That would not be possible if the material developed is cytotoxic and un-inhabitable by the cells. The primary way to assess the biocompatibility of

hydrogels to be used in tissue engineering or as a bioink is to encapsulate them within the 3D hydrogel scaffold and assess their viability, growth, and proliferation.

3.3.1 Cell Culture and Encapsulation

Cells used during all the experiments include NIH-3T3 fibroblasts cell lines that were cultured at 37°C and 5% CO_2 atmosphere. The cell supplementary media used was Dulbecco's modified Eagle's medium (Lonza, Basel, Switzerland) along with 10% v/v heat-inactivated fetal bovine serum (Thermo Fisher Scientific, Waltham, MA), and 1% v/v penicillin-streptomycin (Sigma-Aldrich). The cells were cultured in T75 cell culture flasks (VWR International) and were only used when they were 85-90% confluent.

To characterize the cell viability, cells were encapsulated within the hydrogel scaffold and cultured over 7 days. Hydrogel prepolymer solution of 2% (w/v) 3-day, 5-day, and 10-day MeHA was prepared with EY and TEOA. For instance, a 1mL prepolymer solution of 2% (w/v) 10-day MeHA was prepared by dissolving 0.02g of MeHA in 870 µl of Dulbecco's Sterile PBS (Lonza, Basel, Switzerland) overnight. Once completely dissolved, 10 µl of 100x TEOA (20% w/v) and 20 µl 100x EY (1mM) were added followed by the addition of approximately 3×10^6 cells dispersed in 100 µl PBS. The final prepolymer mixture was pipetted in a 96-well-plate with around 90 µl of the solution in each well. Finally, the cell-laden prepolymer solution was crosslinked through exposure to visible light with help of the DLP-SLA bioprinting system for 5 minutes. Subsequently, the crosslinked cylindrical disks were transferred from the well-plate to a petri-dish, washed with PBS followed by the addition of 5 mL fresh media and incubated at 37 °C and 5% CO_2. Figure 3.3 illustrates the schematic of the entire cell encapsulation process.

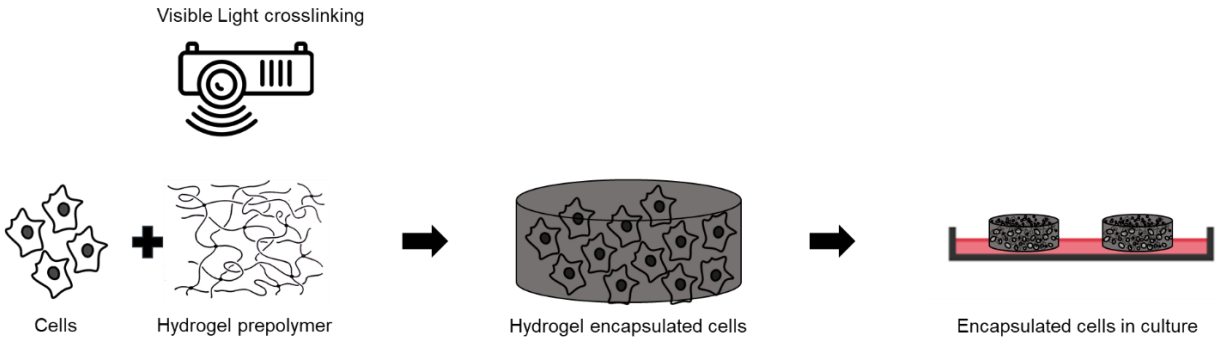

Figure 3.9. Schematic for cell encapsulation strategy using visible light crosslinking.

Once the cells were encapsulated within the hydrogel scaffold, they were then examined for their viability, proliferation, and morphology at days 1, 5, and 7. The cylindrical hydrogel disks were stained with a live/dead assay (Biotium, Hayward, CA), examined, and imaged under a microscope. For each sample at a specific concentration, at least 3 cylindrical disks were analyzed for each day. Briefly, the cylindrical disks were transferred to a 24 well-plate, wash twice with PBS, and incubated with PBS for 15 minutes. Afterward, 500 µl of live/dead assay stock solution prepared with 2mL sterile PBS, 4 µl EthD-III dye in DMSO/H2O, and 1 µl Calcein AM dye in DMSO, was pipetted into the well-plate with the disks and incubated further for 30 minutes. Finally, the samples were examined under an inverted fluorescence microscope (Axio Observer 7, Carl Zeiss Canada Ltd., ON, Canada). A 10x objective lens was used along with the two fluorescent channels (EGFP and mCherry) to capture Z-stacked cross-sectional images of the samples (see Figures 3.4). For simplicity, the EGFP and mCherry channels are referred to as green and red channels respectively.

In order to quantitatively measure the cell viability, the fluorescent images captured with the microscope were processed with ImageJ. First, separate images from each channel (green and red) were exported and converted into an 8-bit gray format. Then the number of live cells was obtained

through image processing using the cell nucleus counter function from the green channel image and recorded. Similarly, the red channel image was used to account for the number of dead cells. Finally, the cell viability was quantified by using the following expression:

$$cell\ viability = \frac{number\ of\ live\ cells(green)}{number\ of\ live\ cells(green) + number\ of\ dead\ cells(red)} \qquad (2)$$

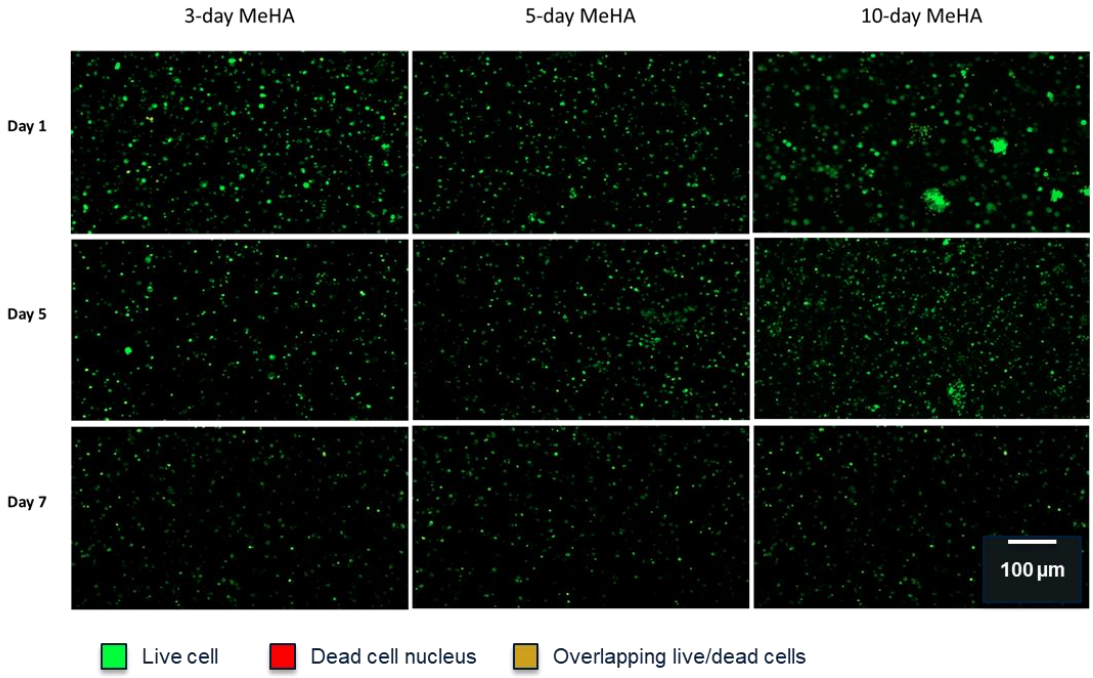

Figure 3.10. A pictomicrograph of encapsulated 3T3 fibroblasts in 3-day, 5-day, and 10-day MeHA

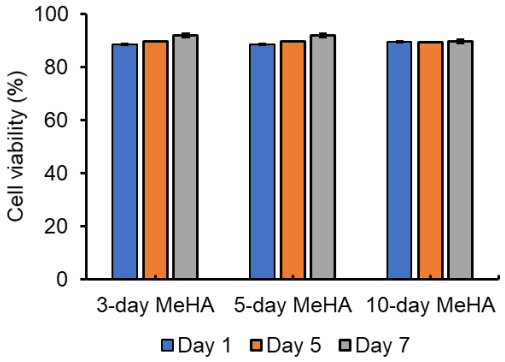

Figure 3.11. Quantitative cell viability of encapsulated 3T3 fibroblasts in 3-day MeHA, 5-day MeHA, and 10-day MeHA.

Cell encapsulation experiments were performed on all three types of MeHA to test for their biocompatibility. The biocompatibility of the hydrogels has to be maintained and should not be affected by any change in other properties as it is uncompromisable. After culturing the encapsulated cells for 7 days, it was observed that all three types of MeHA developed were biocompatible. The cell viability consistently remained above 85% across all samples throughout the 7 days. However, unlike other hydrogels, no change in shape or morphology is observed in any of the samples. This can be attributed to the non-cell-adhesive nature of the HA hydrogel.

3.3.1 Non-cell-adhesive MeHA – a Major Limitation

The primary aim of developing a bioink is to enable the printing of scaffolds for cells wherein they are free to remain and proliferate. Hence, a key criterion for designing bioink is to choose a biocompatible material. Hyaluronic acid is a biocompatible material with no cytotoxic impact on the cells [115]. Moreover, it is known to have bioactive properties and helps with the expression of certain phenotypes in specialized cells. The cell encapsulation study above shows that 3T3 fibroblasts encapsulated in the MeHA scaffold remained viable in the scaffold beyond 7 days

which proves that it is a biocompatible material. However, it was noticed that although the cells remain alive and viable, they do not show any proliferation or change in morphology. Cells within a scaffold are to remain viable but they are also supposed to adhere to the hydrogel matrix, elongate, and proliferate. This is not the case with MeHA hydrogels. As seen through the live/dead assay images, the cell retained the shape of their nuclei and remained unattached to the scaffold. They were seen to remain in clusters and no attachment was noticed even after 7 days. This trend noticed in MeHA is due to its non-cell-adhesive nature [122,137]. The MeHA polymer chains lack the presence of cell-adhesive motifs. Cells tend to interact with relatively positively charged amine groups and attach through protein-integrin interactions. Therefore, due to the lack of cell-adhesive motifs, it is not possible for cells to attach to the hydrogel matrix and proliferate. This is one of the most important reasons why the use of MeHA is often seen in combination with other cell-attachable motifs or biomaterials. This is a major limitation for the developed methacrylated hyaluronic acid-based hydrogel that needs to be addressed.

3.4 Chapter Summary

In Chapter 3, the developed 3-day, 5-day, and 10-day MeHA is characterized and evaluated. The effect of the duration of the synthesis is confirmed through the NMR analysis which validates the reaction mechanism. Furthermore, the compressive modulus of the three types of MeHA reflects the importance of DS in developing a mechanically stiff scaffold. Through the evaluation of the DS, viscosity, and mechanical property, a clear picture is painted which would help researchers optimize the proposed synthesis protocol per their need. Finally, the biocompatibility study reveals that although all types of MeHA synthesized were biocompatible, however, due to the lack of cell-adhesive motifs cells do not proliferate within the hydrogel scaffold.

Chapter 4: Cell-attachable GelMA-MeHA Hybrid Bioink

Chapter 4 introduces the use of the well-known photocrosslinkable biomaterial Gelatin methacryloyl (GelMA) with MeHA. GelMA as a hybrid component in the MeHA bioink can introduce cell-adhesive properties in the hydrogel matrix. In addition to the cell-adhesive properties, the use of GelMA can enable enhanced 3D bioprinting with MeHA through its advantageous properties. Therefore, the hybrid GelMA-HA hydrogel is further characterized in terms of its mechanical properties, surface microarchitecture, and biocompatibility.

4.1 Synthesis of Gelatin Methacryloyl (GelMA)

The synthesis of Gelatin methacryloyl (GelMA) was done by following the protocol reported in Kumar *et al* [138]. In short, 5 g of powdered gelatin from porcine skin (Type A, Bloom strength 300, Sigma-Aldrich, St. Louis, MO, USA) was dissolved in 50 mL of reverse osmosis purified (RO) water. The gelatin was allowed to completely dissolve in the solvent and the pH of the solution was adjusted to 9 by using sodium hydroxide (NaOH). Following the pH adjustment, 9 mL of glycidyl methacrylate (GM) (Sigma-Aldrich) was added dropwise to the gelatin solution. Then the solution was kept at 50°C with constant stirring at 500 RPM for 12 hours. Once the reaction was complete, the solution was diluted with 50mL of RO water, transferred to dialysis tubing (12-14 kDa) (Fisher Scientific, Waltham, MA, USA) and dialyzed against RO water for 3 days. It was ensured that the water was changed twice every day until completion. After the completion of dialysis, the filtered solution was then frozen at -20°C and then lyophilized to obtain foamy solid GelMA. The final GelMA product was then stored at -20°C for future use. The schematic below shows the reaction taking place during the GelMA synthesis reaction. In one reaction pathway, the hydrolysis of Glycidyl Methacrylate (GM) takes place which can be

substituted and grafted on the gelatin chain through replacement of a) primary amine groups and b) hydroxyl group. However, in another pathway, the GM can undergo an epoxide-ring opening hence result in the substitution of c) hydroxyl groups and d) primary amine groups.

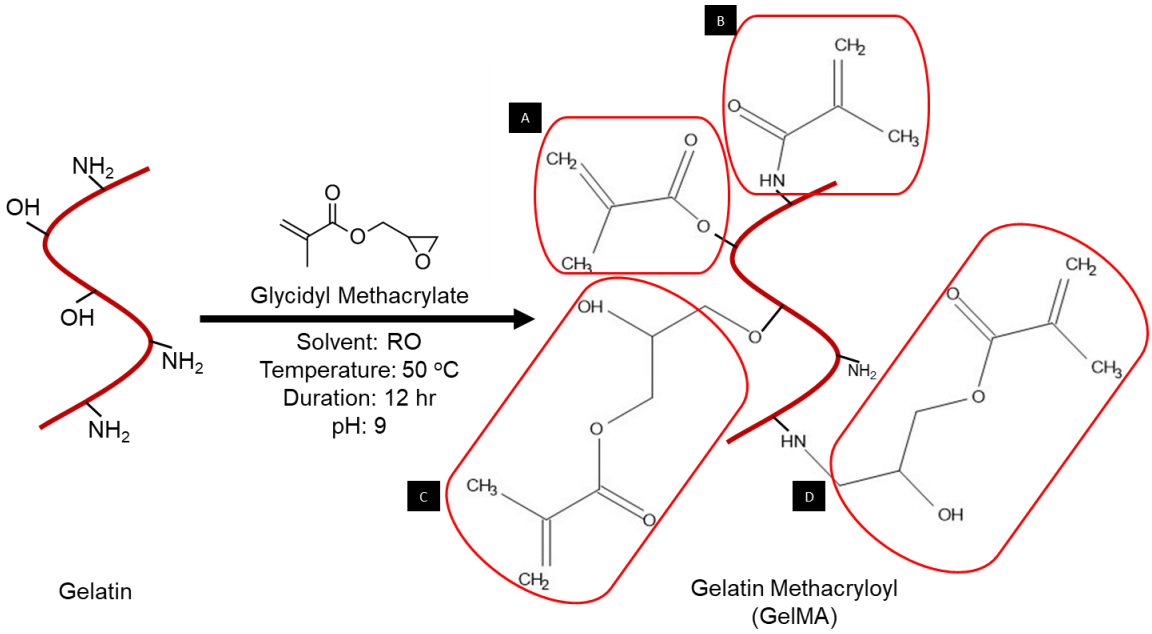

Figure 4.12. Schematic for the reaction mechanism of GelMA with possible outcomes of substitution reactions is annotated by (A), (B), (C), and (D). (Adopted from [138])

The DS for the GelMA synthesized with the protocol suggested above was then analyzed with ^{1}H NMR. The NMR spectra obtained show the methacrylate vinyl group at 6-6.2 ppm and 5.6-5.8 ppm and the GM methyl at 1.8 ppm. These groups being present on the spectra proves that substitution has taken place. To calculate the DS, the decrease in the signal of primary amines at 2.8 – 2.95 ppm were compared with phenylalanine at 7.0-7.5 ppm. The relative integration of the peaks revealed a DS of 90% with the GelMA [138]. The high DS, along with a very low viscosity adds great value to the hybrid bioink. As a result of the high DS, a noteworthy contribution in the

mechanical strength and crosslinkability can be expected without barely affecting the net viscosity of the hybrid bioink.

4.2 Preparation of GelMA-MeHA Hybrid Bioink

To investigate the influence of GelMA hydrogel to enable cell attachment within the hydrogel matrix of MeHA, different combinations of the hybrid hydrogel was prepared and examined. GelMA as a component of the hybrid bioink promises more than only cell attachment. It can be expected to impact the mechanical strength, pore microarchitecture, and swelling characteristics. Keeping these into consideration, the proportion of GelMA was varied while keeping the MeHA constant. One-fold, two-fold, and three-fold GelMA was combined with 2% MeHA and examined. The following table shows the different proportions of the hydrogel used during the experiment.

Table 4.3. GelMA-MeHA hybrid bioink preparation and experiment plan.

	3-day MeHA	*5-day MeHA*	*10-day MeHA*
Group 1	2% GelMA 2% MeHA (2G $2HA_3$)	2% GelMA 2% MeHA (2G $2HA_5$)	2% GelMA 2% MeHA (2G $2HA_{10}$)
Group 2	4% GelMA 2% MeHA (4G $2HA_3$)	4% GelMA 2% MeHA (4G $2HA_5$)	4% GelMA 2% MeHA (4G $2HA_{10}$)
Group 3	6% GelMA 2% MeHA (6G $2HA_3$)	6% GelMA 2% MeHA (6G $2HA_5$)	6% GelMA 2% MeHA (6G $2HA_{10}$)
Control	2% MeHA ($2HA_3$)	2% MeHA ($2HA_5$)	2% MeHA ($2HA_{10}$)

The hybrid hydrogels were prepared very similarly to the preparation as described in Chapter 2.4.1. Briefly, a 1 mL precursor solution of $(6G\ 2HA)^{10}$ was prepared by dissolving 0.06 gm

GelMA and 0.02 gm MeHA in 970 µl PBS. The solution was then vortexed overnight to completely dissolve and finally, 10 µl of 100x TEOA (20% w/v) and 20 µl of 100x EY (1mM) were added for visible light crosslinking. If the hydrogels were used in the experiment with cells, then it was dissolved in 870 µl of PBS, and cells were added as a dispersion in 100 µl PBS to ensure the concentration remains unchanged.

Previous studies have well elucidated the characteristics of GelMA, therefore it was not the focus of the thesis. The biocompatibility studies were performed with all three types of MeHA produced. However, since 10-day MeHA exhibits the best mechanical properties hence compressive modulus, swelling characteristics, and pore microarchitecture of the hybrid bioink were only examined with 10-day MeHA.

4.3 Characterization of GelMA-MeHA Hybrid Bioink

In order to examine the mechanical properties of the GelMA-MeHA hybrid hydrogels. The crosslinked hydrogel samples were used to measure the compressive modulus using the Hertz contact mechanics model as described in Chapter 3.2.1. It was expected that due to the introduction of GelMA with the MeHA hydrogel, the mechanical strength, and structural integrity would be improved. GelMA has always been reported to have significantly higher DS and compressive modulus in comparison to MeHA [122].

4.3.1 Mechanical Strength

The results from the compressive modulus tests with the GelMA-HA hybrid hydrogel show significant improvement as shown in Figure 4.2. The compressive modulus of 10-day MeHA was only about 2.44 kPa (See Chapter 3.2.1, Figure 3.2) which had almost doubled to 4.8 kPa due to

the addition of just 2% GelMA. Moreover, an increasing trend is noticed as the concentration of GelMA increases. With the use of 6% GelMA, the compressive modulus reached a maximum of 10.8 kPa. This shows that the introduction of GelMA greatly enhances the mechanical stiffness of the hydrogel. Moreover, since the stiffness of the hydrogel substrate is often key to cell behavior including cell attachment, morphology, and phenotype expression, therefore this improvement can be a decisive factor in the hybrid bioink [139]. The enhancement of mechanical strength should not only be attributed to GelMA. It is a result of combined contributions from MeHA and GelMA. Studies report that 6% pristine GelMA to have a compressive modulus of around 6.6 kPa [80]. The GelMA-HA hybrid hydrogel exhibits an increase of almost 55% to this reported value. The statistical comparison between the 4 samples examined portrays that the difference in the mechanical property of the samples is significant with the confidence of $p < 0.0001$. It can be attributed to the greater crosslinking density inside the scaffold due to the availability of more polymer chains and methacrylate groups [140]. Since two different types of methacrylated hydrogels are used, this means that there is a greater number of sites for the free radicals to attack and bind resulting in greater crosslinking density. In addition to that, there is an influence due to inter-species attraction and bonding between two polymer types as well.

This enhancement of the mechanical stiffness of the GelMA-HA hybrid hydrogel is the combined synergistic contribution of both. It shows that when combined they can make a noteworthy enhancement to each other's properties. Hence, together, they are an effective tissue engineering tool.

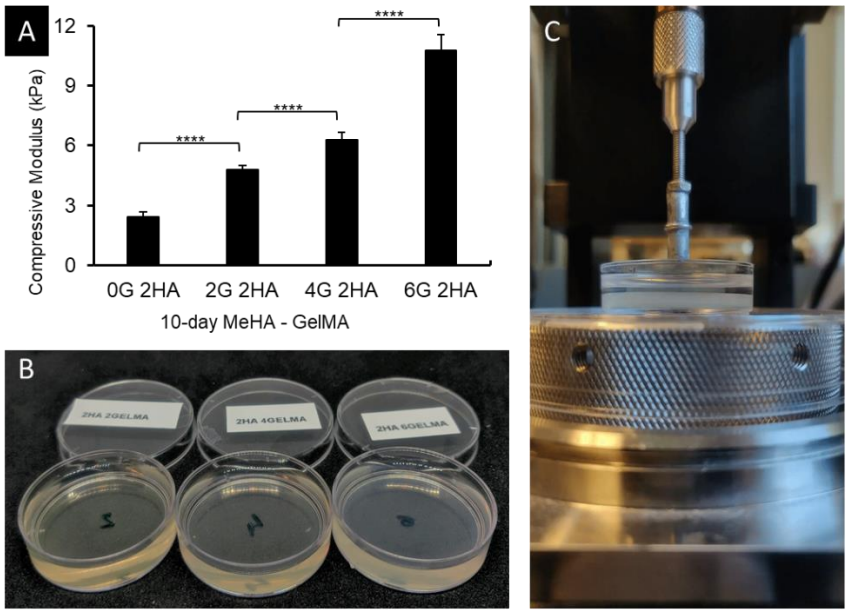

Figure 4.13. Mechanical properties of GelMA-MeHA hybrid hydrogel. (A) Compressive modulus of a different combination of GelMA-MeHA hybrid hydrogel. (n = 10; * $p < 0.05$, ** $p < 0.01$, *** $p < 0.001$ and **** $p < 0.0001$). (B) Crosslinked hybrid hydrogel samples used for mechanical tests. (C) Testing compressive modulus of samples using vertical axis mechanical tester.

4.3.2 Swelling Ratio

Measuring the swelling ratio of the crosslinked hydrogel samples helps to understand the relative degree of crosslinking and the water uptake capability. To describe the procedure briefly, prepolymer solutions were prepared as described in Chapter 2.4.1 and poured into a 24-well plate. Approximately 0.5 mL precursor solution was used for a single sample and crosslinked under visible light using the DLP-SLA 3D bioprinter. Subsequently, the crosslinked hydrogels were immersed in PBS and kept in a 37°C incubator for 24 hours. Once fully hydrated, each sample's hydrated weight was recorded. Afterward, they were frozen in a -20°C freezer and lyophilized for 2 days before their dry weight was measured again. Finally, the following equation was used to calculate the swelling ratio:

$$Swelling\ ratio = \frac{Swollen\ weight}{Dried\ weight} \quad (3)$$

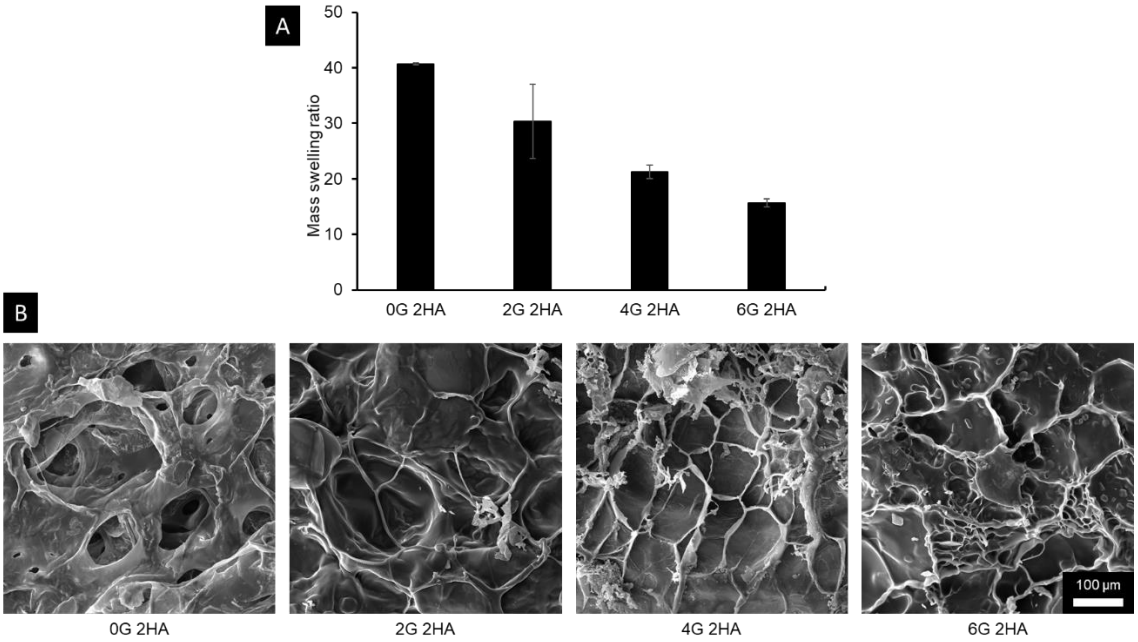

Figure 4.14. Mass swelling ratio and surface microstructure of GelMA-MeHA Hybrid hydrogel. (A) Mass swelling ratio of all combinations of GelMA-MeHA hybrid hydrogel. (n = 5) (B) Scanning Electron Microscopy (SEM) images illustrating the porous microstructure of GelMA-MeHA hybrid hydrogel.

The ability to retain water within the hydrogel matrix is an important criterion for its use in tissue engineering applications. Hydrogels enable the mimicking of the native environment through its ability to hold water and adsorb several proteins in the process. However, water retention ability comes with a tradeoff – the stiffness of the hydrogel matrix. Stiffer hydrogels are not able to hold more water; therefore, the swelling ratio is expected to have an opposite trend compared to the compressive modulus results. Figure 4.3A shows that the results from the swelling ratio are as expected. The $(2HA)_{10}$ samples have the highest swelling ratio. Its hydrated weight is

40 times more compared to its dehydrated weight. The water retention capability decreases as the hydrogel becomes stiffer hence $(6G\ 2HA)_{10}$ samples show $3/8^{th}$ of the water retention capacity compared to $(2HA)_{10}$.

4.3.3 Microstructure Architecture

To investigate the surface microstructure of the GelMA and MeHA hydrogel, scanning electron microscopy (SEM) was used. For this characterization, 2 mL hydrogel precursor was prepared for each hydrogel group at defined concentrations as described in section 4.2, crosslinked with visible light, and hydrated with PBS in the 37°C incubator for 24 hours. Subsequently, they were frozen in a -20°C freezer and lyophilized for 2 days. The lyophilized samples were then sputter-coated with Pt/Pd alloy (80% Pt and 20% Pd) and imaged using the SEM (Mira3 XMU, TESCAN, Brno, Czech Republic).

Figure 4.3B shows the pore microstructure of the 10-day MeHA hydrogel samples and the GelMA-HA hybrid hydrogel samples. The SEM images are a good way to investigate the surface characteristics and porosity of a hydrogel. It is vital because porosity can be linked to several important factors including cell growth, hydrogel matrix stiffness, and is also known to affect the diffusion of substances within the hydrogel matrix [141]. Although different cell types have varied requirements for optimum cell growth and proliferation, some reports suggest that stiffer hydrogel matrices with larger pore sizes lead to better cell proliferation [142]. Previous studies report typical pore diameter of around 100-150µm for GelMA and pore diameter of around 150 µm is also reported in studies for HA [143,144].

Observations show that 2% MeHA hydrogel pores do not have a very definitive shape. The boundaries are not definitive with no or less clear distinctions. It can also be representative of the

fact that its mechanical properties are significantly low compared to GelMA. However, as GelMA is introduced as a component with MeHA, changes in the definition of the pores are observed. Only with the introduction of 2% GelMA to the 2% MeHA, the pore structure starts to become more definitive which is further enhanced with the introduction of 4% and 6% GelMA. The sample with 6% GelMA shows a pore that is most definitive with clear boundaries and can be attributed to its mechanical strength as well. Moreover, this definitiveness of the pore and the resulting stiffness of GelMA can also be one of the reasons why it provides a better environment for cell attachment. Surface stiffness affects different cells in different ways and fibroblast cells are more likely to spread on surfaces with higher stiffness [139]. These microstructure images provide a clear idea of the changes taking place within the hydrogel matrix at the microscale due to the addition of GelMA. These images were not used to calculate the pore size of the hydrogel because lyophilization is known to affect the pore geometry hence only previously reported data is utilized as a measurement metric.

4.3.4 Biocompatibility

In order to assess and evaluate the biocompatibility of the hybrid hydrogel, cell encapsulation experiments were performed with all combinations in Table 4.1. As described in Chapter 3.3, the live and dead assay was performed on days 1, 5, and 7 and finally, the cell viability was calculated. Besides, to investigate the cell attachment and cell morphology, the encapsulated samples were stained with Phalloidin (Cytoskeleton, Denver, CO, USA) and 4’,6-diamidino-2-phenylindole (DAPI) (FluoroshieldTM with DAPI, Sigma-Aldrich) for cytoskeleton and nuclei staining respectively after 14 days of culture. Briefly, the cylindrical hydrogel samples were washed with PBS and transferred to a 24-well plate. 500 µl of 3.7% (v/v) paraformaldehyde was added for 30

minutes to fix the cells. Subsequently, 500µl of 0.5% (v/v) Triton X-100 in PBS(Sigma-Aldrich) was added for 10 minutes to make the cell membrane permeable. Next, 500 µl of 100nM phalloidin 488 stock solution was added to the samples and incubated at 37°C for 60 minutes. Next, the samples were washed thrice with PBS before adding 500µl DAPI stock solution for 10 minutes. Finally, the samples were imaged with a 10x and 20x objective lenses in an inverted fluorescence microscope with DAPI and EGFP channels in Z-stack mode.

Figure 4.4 shows the encapsulated hydrogel samples just before the preparation of cytoskeleton and nuclei staining. It is noteworthy to observe the shape fidelity of the hydrogels with varying GelMA concentration. Samples with high GelMA content are able to retain their shape better compared to other samples.

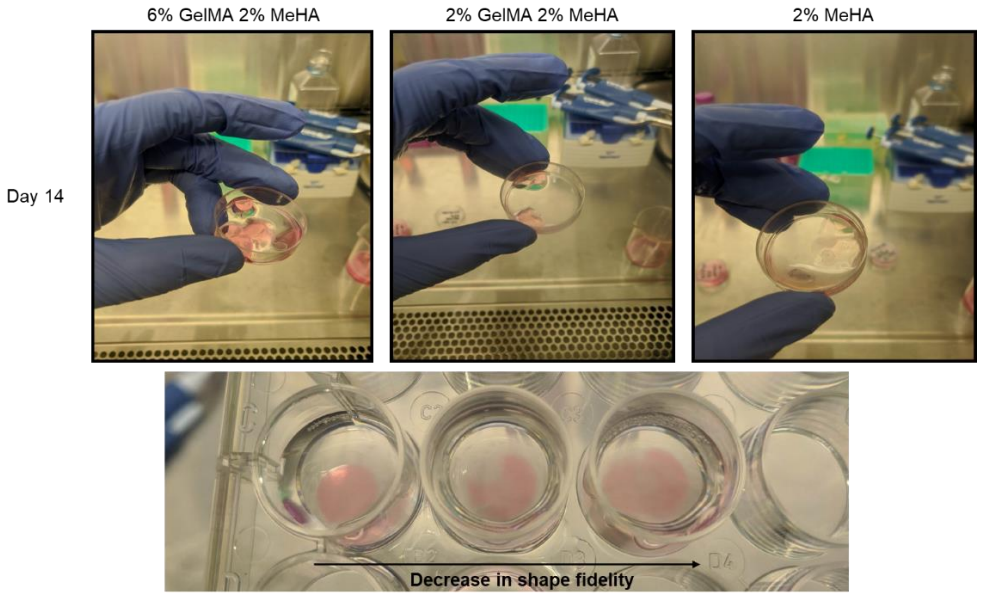

Figure 4.15. GelMA-MeHA hybrid hydrogels with 3T3 fibroblast cells encapsulated in culture

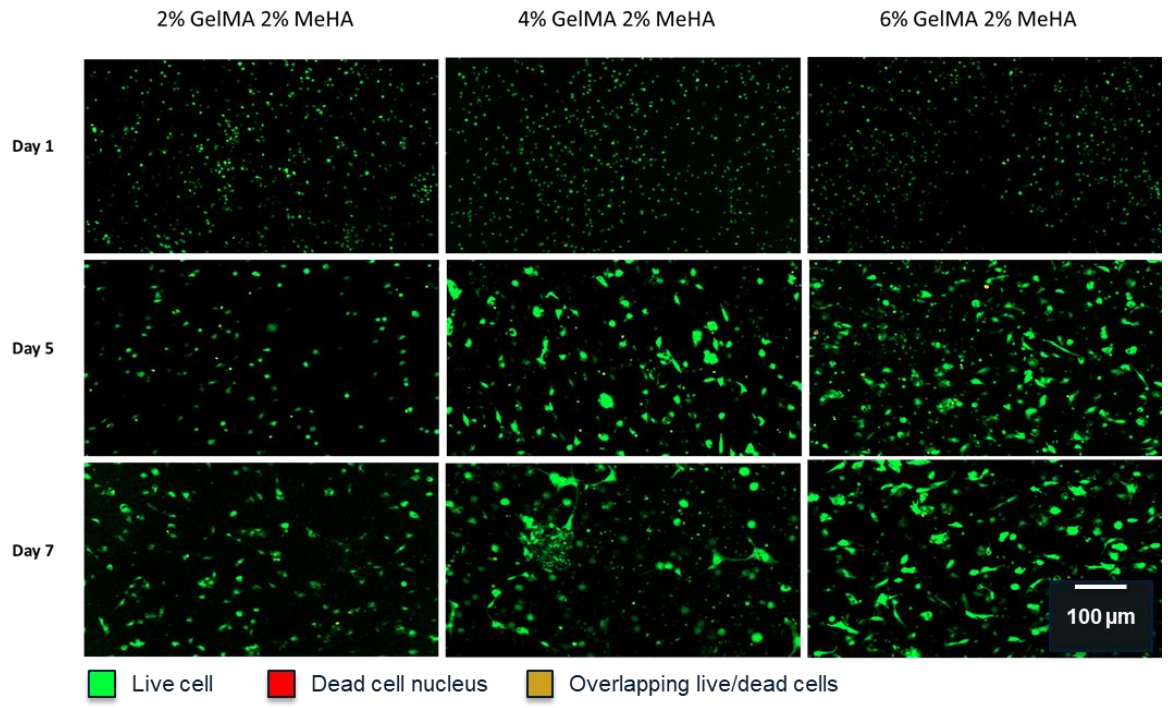

Figure 4.16. Photomicrograph of encapsulated 3T3 fibroblasts in GelMA-MeHA hybrid hydrogel. Green represents the cell bodies of the live cells.

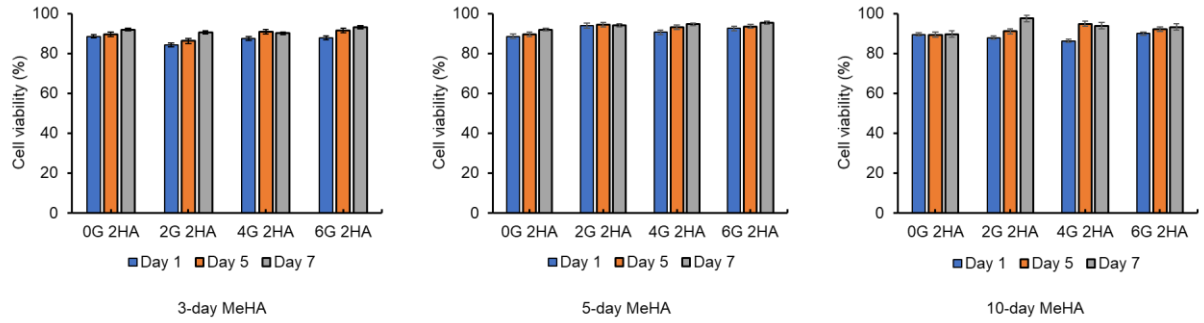

Figure 4.17. Cell viability of encapsulated 3T3 fibroblasts in GelMA-MeHA hybrid hydrogel with (A) 3-day MeHA (B) 5-MeHA and (C) 10-MeHA

The cell studies with 3 different types of MeHA combined with GelMA show that all the tested samples were biocompatible. The cells encapsulated in all the variants remained alive and viable throughout 7 days and up to 2 months (data not shown). During the 7 days, the cell survival

rate remained about 85% for all samples and noticeable cellular attachment and elongation were evident. Although live and dead assay is not the standard for illustrating cell attachment, it can reflect when the cell morphology changes significantly. From day 5 onwards, cell elongation is noticeable which becomes more evident on day 7. It can also be noticed that the samples with more GelMA had more changes in cell morphology. The increased concentration of GelMA within the hydrogel matrix results in the availability of more cell-binding amine groups along the whole polymer chain. Therefore, in samples with higher GelMA concentration, the cell starts to attach and change their morphology rapidly [76]. The encapsulated cells were continued to be cultured for over 2 months to observe the cell attachment and morphology. As time passed, the degradation of the samples was noticed. Due to its poor mechanical stiffness, 3-day MeHA and its hybrid samples lost its shape fidelity fastest compared to the others. On the other hand, 10-day MeHA samples performed significantly better and retained their shape most successfully.

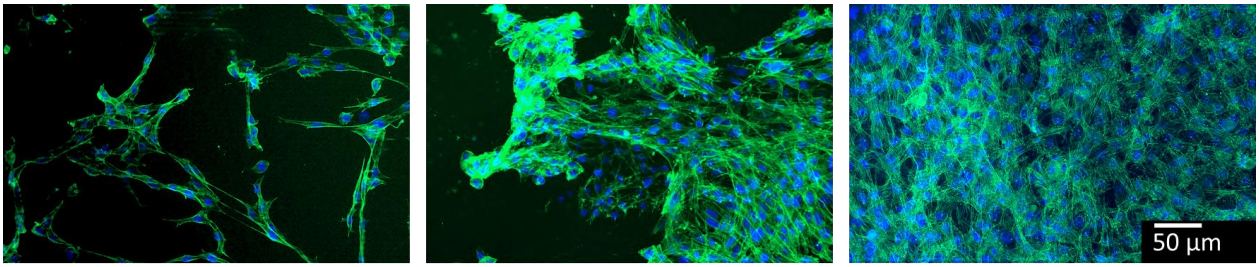

(A) 2% GelMA 2 MeHA (B) 4% GelMA 2% MeHA (C) 6% GelMA 2% MeHA

Figure 4.18. Fluorescent images of various portions of 3D encapsulated samples showing cell morphology after 14 days of culture with F-actin (green: Phalloidin) and nuclei staining (blue: DAPI)

4.4 DLP-SLA 3D Bioprinting

The development of the hybrid bioink is carried out so that it maybe be used to bioprint scaffolds for applications in biofabrication techniques. Therefore, it is the amalgamation of the

efforts made in the previous chapters. Although there has been some application of extrusion-based bioprinting with MeHA, however, DLP-SLA-based 3D bioprinting, to our knowledge, is the first of its kind.

4.4.1 DLP-SLA Bioprinting System

One of the strongest aspects of the bioprinting system used in this thesis is that it can be assembled just by using off-the-shelf components without the need for much modification. The key component utilized is a projector. It consists of a micromirror array that is made by microfabrication and is referred to as the Digital Micromirror Device (DMD). Each micromirror on the DMD is essentially a pixel that reflects the light from the illumination source onto the projection plane. It can control the intensity of the pixel through a change in the angle of the micromirror, therefore, resulting in pixels with different intensity. Figure 4.8 (B) illustrates the mechanism of how pixel intensity is varied by the DMD. The black area represents the low-intensity pixel whereas the green area is the high-intensity pixel. The projected light passes through the lens used by the project, through the water filter system on to the vat containing the hydrogel. As elucidated earlier, the water filter system eradicates the harmful aspects of the projected beam after which the high light intensity areas of the hydrogel vat are crosslinked due to the reaction triggered by the photo-initiator present. The introduction of the high-intensity light onto the hydrogel vat starts a chain reaction, which results in the production of free-radicals; hence it is photopolymerized, unlike the areas without high-intensity light exposure. Therefore, with the utilization of an off-the-shelf project system, it is possible to selectively crosslink hydrogel with any given pattern in a layer-by-layer manner.

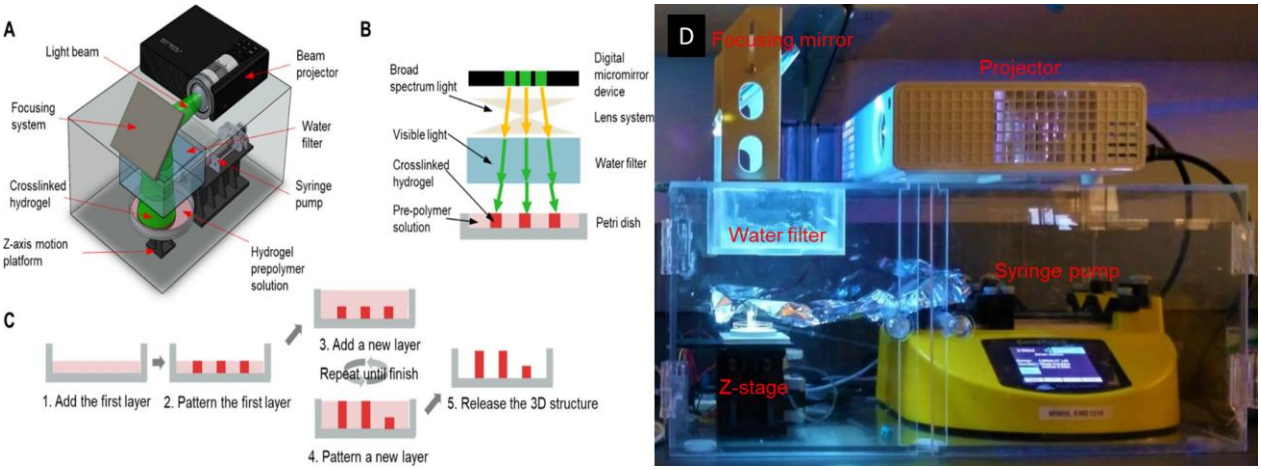

Figure 4.19. (A) Schematic of DLP-SLA 3D bioprinting setup (B) Illustration of selective crosslinking of hydrogel utilizing the DMD array (C) Printing steps for fabricating large 3D scaffolds using DLP-SLA bioprinting (Adopted from [145]) (D) Actual Image of the DLP-SLA 3D bioprinting setup used

The plane of printing of the projector system is about 9.6 cm × 5.4 cm, which typically results in printed feature size of around 50 μm per pixel [146]. A projection angle of around 12° exists between the projection angle and the axis, along with some degree of distortion resulted due to refraction from the presence of the water filter. Therefore, the whole printing setup was first calibrated and during the printing process the focal plane of the projector was adjusted after each layer was completed [146].

In order to understand the printing process for a large 3D printed structure, it is necessary to understand that the 3D SLA printing process is a layer-by-layer printing method. To describe it briefly, once the crosslinking or patterning of the first layer is completed, another layer of hydrogel prepolymer solution is dispensed by the syringe pump, and sequentially, the 2nd layer is crosslinked. This process is repeated until a whole 3D structure is formed as illustrated in Figure 4.8 (C). Throughout the process, it is necessary to control the time that is allowed for crosslinking

of each layer to avoid under or over-crosslinking. Lastly, after the completion of the printing process, any un-crosslinked prepolymer is washed with PBS and removed from the petri dish.

4.4.2 GelMA-MeHA Hybrid Bioink Preparation

To bioprint structures with the SLA bioprinting setup, prepolymer solutions were prepared as described in Chapter 3.3. Briefly, 3T3 fibroblast cells cultured were detached with trypsin, centrifuged to a pellet, and evenly mixed with a prepolymer solution of a specific concentration. Approximately, 8×10^6 cells were used per mL of 4% GelMA and 2% HA solution. Two shapes were fabricated which included - a flower with petals and a lung model. Once the hydrogel prepolymer was prepared with cells, the structures were printed with the help of the SLA bioprinting setup in a layer-by-layer fashion and any un-crosslinked hydrogel was washed and removed with PBS. After washing, fresh cell growth media was added to the printed structures, and they were left to culture in the incubator at 37°C and 5% CO_2 atmosphere. Similarly, the bioprinted samples were then examined for their cell attachment using the cytoskeleton and nucleus staining with Phalloidin and DAPI as described previously in Chapter 4.3.

The printed flower scaffold has a dimension of 15 mm in length, 15 mm in width, and 2 mm in thickness. Similarly, the miniature lung model is 15x20x2 mm along the length (vertical), width (horizontal), and thickness respectively. Both the samples were crosslinked with visible light exposure for 5 minutes. Upon completion of SLA bioprinting, the printed scaffolds were cultured and then imaged for cell attachment and proliferation after day 5. Through observation, the mechanical integrity of the printed structures remained consistent and no major change in shape fidelity was observed. A slight variation of the height observed in D is due to a minimal slant of the printing plane during printing. The printing resolution is noteworthy because bioprinting with

MeHA is not known for high-resolution bioprinting[117]. Considering this, the structural integrity and mechanical strength of the bioprinted scaffolds were promising.

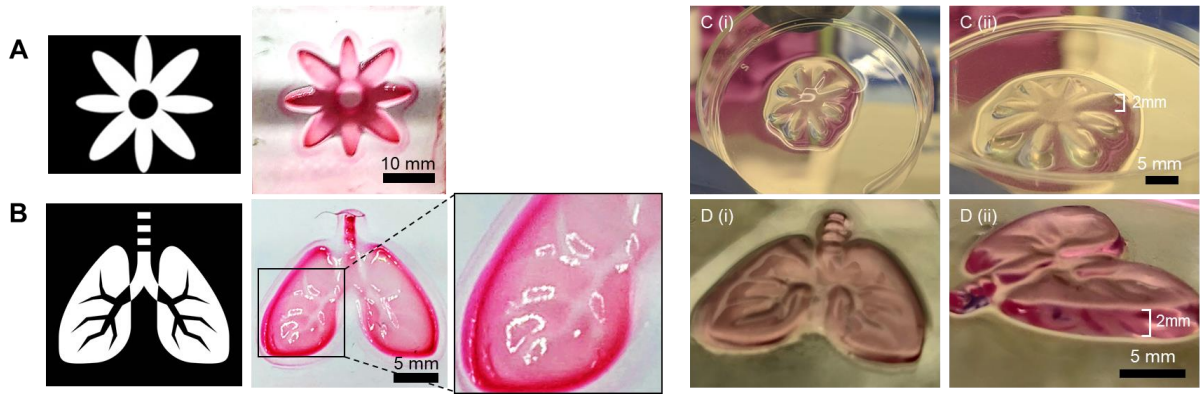

Figure 4.20. Bioprinted scaffolds without cells (A) Flower model (B) A miniature lung model. The fabricated samples in (A) and (B) were stained with red food-dye for better visualization. (C) and (D) shows printed bioprinted scaffolds with 3T3 cell encapsulated.

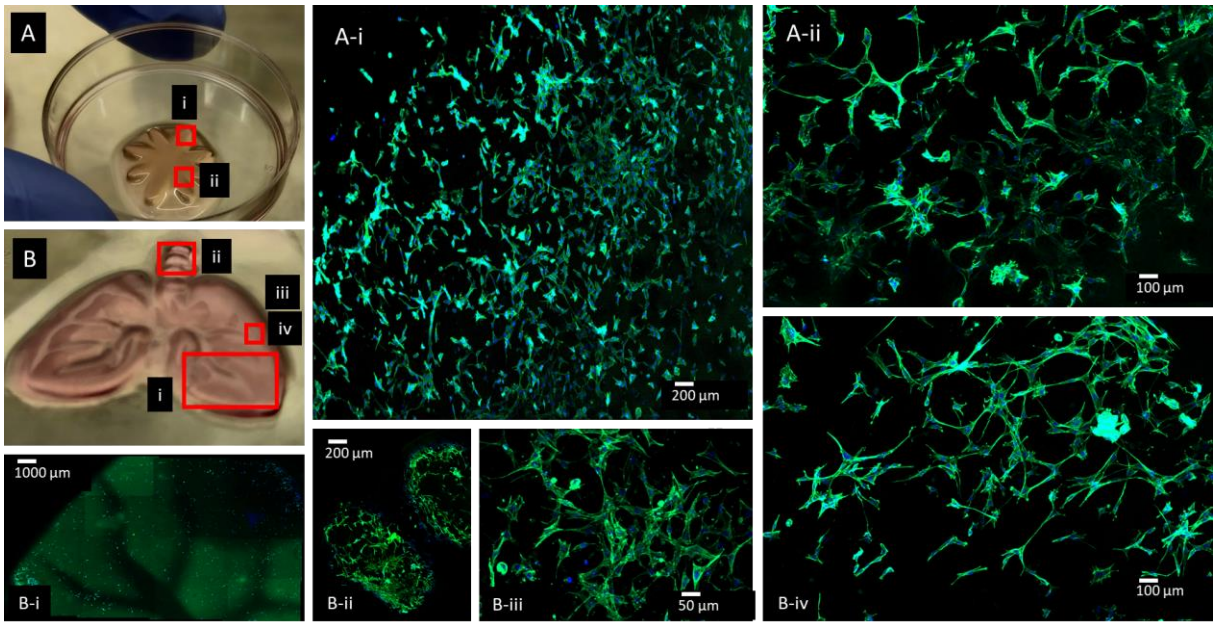

Figure 4.21. Fluorescent images of various portions of bioprinted scaffolds showing cell morphology after 5 days of culture with F-actin (green: phalloidin) and nuclei staining (blue: DAPI)

The cytoskeleton and nuclei stained images show that cell attachment and proliferation took place within the bioprinted scaffold. Images with 5x, 10x, and 20x magnification show cell attachment and proliferation all over the scaffold with different perspectives. The highest cell attachment, dense tissue-like formation, and proliferation are noticed at the boundaries of the structures. It is a well-known phenomenon due to the availability and easier diffusion of growth media near the boundaries. Figure 4.9 shows the top and perspective view of the printed scaffolds with cells. The 5x magnification images give an overview of the cell population throughout the structure whereas the 10x and 20x magnification images provide a closer view of the cell morphology. For instance, Figure 4.10 (B) (i) shows that the cells are well attached and are starting to show proliferation along the boundary of the vasculature pattern. In addition to that, only encapsulated cells within the hydrogel are proliferating and starting to form an almost tissue-like scaffold. Moreover, Figure 4.10 (B) (iv) shows that the stained cartilage portions of the lung model. It can exhibit that selective crosslinking of the hydrogel took place, therefore, cells were only encapsulated where they were meant to be and that there is no or very less unwanted crosslinking taking place through DLP-SLA bioprinting.

The bioprinting was carried out with $(4G\ 2HA)^{10}$ hydrogel, it was selected among the other concentrations because its mechanical strength, swelling characteristics, and biocompatibility were significantly improved in comparison to 2% MeHA but it was the most stiff with the least water retention capability. Bioprinting with this particular sample shows that if required, better resolution, faster crosslinking and mechanical strength and integrity can be obtained if $(6G\ 2HA)^{10}$ is used. Therefore, it lays the groundwork for future optimization and application of DLP-SLA bioprinting with GelMA-HA hybrid bioink.

4.5 Chapter Summary

This chapter focuses on overcoming the major limitation, non-cell adhesiveness of MeHA, through the introduction of cell adhesive GelMA hydrogel. The hybrid cell-adhesive hydrogel is then characterized in terms of its mechanical properties and biocompatibility. After a complete characterization, the hybrid hydrogel is used to bioprint miniature models using a DLP-SLA bioprinting system. The bioprinted miniature scaffolds show that 3T3 mouse fibroblasts can remain viable, attach, and proliferate well within the hybrid hydrogel.

Chapter 5: Conclusion

5.1 Concluding Remarks and Future Perspectives

The primary aim of the work presented in this thesis involves the development of a biomaterial that is suitable for tissue-specific applications with 3D bioprinting methods. The prevalence of hyaluronic acid in the extra-cellular matrix makes it a suitable material for mimicking the native microenvironment along with several specific advantages like cell proliferation and differentiation due to its biological properties. Hence, this thesis focuses on the development of a hydrogel scaffold with hyaluronic acid due to its significant advantages, especially in tissue-specific applications.

The development of a photo-crosslinkable hyaluronic acid hydrogel in the first objective is key to enabling its use with existing 3D bioprinting systems. A common thread between existing 3D bioprinting systems involves crosslinking the bioink post-printing, which is often achieved through the use of a light source. Often, biomaterials are chemically modified with methacrylate groups to enable the capabilities of photocrosslinking. Despite significant challenges, as discussed in section 2.2, the protocol developed in this thesis is able to produce methacrylate hyaluronic acid (MeHA) along with one of the highest DS, which is able to photocrosslink while maintaining its structural integrity.

The MeHA with 3 different degrees of substitution (32%, 42%, and 88%) were achieved through varying the duration of synthesis. The different degree of substitution (DS) resulted in varied viscosity, crosslinking time, and mechanical properties. It was observed through the characterization of the 3 different types of MeHA that the highest DS resulted in the shortest crosslinking time, low viscosity, and superior mechanical properties. Therefore, through this protocol, a premise of synthesizing MeHA with tunable DS depending on the requirement of the application was established. Besides, the synthesized MeHA was demonstrated to crosslink

successfully at 37ºC, the core temperature of the human body, within 30 minutes using a thermally activated initiator. This capability can be used to utilize MeHA as a wound-healing material with the ability to crosslink *in-situ* on the human body. Moreover, it can be used to further enhance the mechanical strength of 3D bioprinted scaffolds through dual crosslinking methods.

In addition to dual crosslinkability, the synthesized hydrogel scaffold was able to demonstrate its biocompatibility with 3T3 fibroblasts. The encapsulated cells remained viable throughout the period of observation hence validating the biocompatibility of the scaffold. However, by virtue of HA's non-cell-adhesive nature, there was no cell attachment noticed throughout the scaffold, which was addressed in the second objective.

Through the implementation of the second objective, this non-cell adhesive nature of the MeHA hydrogel was addressed with the incorporation of cell-adhesive bioink Gelatin methacryloyl, GelMA. This averts any further chemical modification of MeHA with cell-adhesive motifs and also enables the use of 3D-bioprinting friendly characteristics of GelMA. The evaluation of the hybrid GelMA-HA bioink shows that GelMA not only allows cell attachment with good biocompatibility but it also greatly enhanced the combined structural strength and fidelity.

The development of MeHA was targeted to enable its application in DLP-SLA-based 3D bioprinting. The approach to developing a hybrid cell-adhesive hydrogel with GelMA, not only addressed the limitation of MeHA in terms of cell attachment but also with bioprintability. DLP-SLA bioprinting was carried out with GelMA-HA hybrid hydrogel which shows promise in terms of its printing resolution, crosslinking capability, and biocompatibility along with cell-attachment. Through the use of the hybrid bioink, there may be a way to address previously reported lacking such as poor mechanical properties and resolution with the use of only MeHA [147]. Therefore,

the developed hybrid bioink is not only able to utilize the DLP-SLA system for attaining much-enhanced resolution, shorter printing time, but also leverage tissue-specific advantages due to the availability of HA within the scaffold.

Over the past decade, biofabrication techniques have evolved to offer a promising solution for the lack of replacement tissues for study and therapy. These methods are now closer to developing well-controlled heterogeneous cellular microenvironments and mimicking structural and functional intricacies that are present *In vivo*. So far, these techniques have been employed to generate several artificial tissues, that have been both, implanted *In vivo* and used for *in-vitro* disease studies.

Therefore, considering the wide range of applications and scope for biofabrication techniques like 3D bioprinting in the future, there needs to be a greater focus on the development of compatible biomaterials. Biomaterials that can mimic native conditions more effectively while maintaining its printability properties. The greater the degree of congruency to *In vivo* condition is achieved, the further the technology will progress in the development of heterogeneous and functional constructs. It will allow researchers and medical practitioners to study cell biology more effectively, screen drugs to a greater capacity *in-vitro*, and allow avenues for organ or prosthetic transplant in the future. This can only be achieved through the use and characterization of native and naturally derived substances like HA and gelatin for biofabrication purposes.

Overall, the field of biofabrication is advancing at a rapid pace. As we move forward in the post-pandemic world, there would be a greater emphasis on the advancement of bioengineering. Existing biofabrication techniques aided with additive manufacturing technologies have enabled the development of promising complex biological structures. Through the development of new biomaterials, this progress can be spearheaded in the right direction. As this emerging

interdisciplinary field of science and engineering advances, there will be daunting challenges, but these small incremental additions keep the hopes and aspirations alive.

5.2 Contributions

Methacrylation of hyaluronic acid has been a challenging avenue for many researchers involved in 3D bioprinting. The contribution made through this thesis is as follows:

1. A stable protocol for the methacrylation of hyaluronic acid was developed to obtain tunable DS based on the length of synthesis. 88% DS obtained with 10-day MeHA is one of the highest reported in the literature.
2. Thermal crosslinking of MeHA was introduced to enable dual-crosslinkability with DLP-SLA 3D Bioprinting.
3. MeHA with 3 different DS (high, moderate, low) was characterized in terms of biocompatibility, mechanical property, and bioprintability.
4. First-ever DLP-SLA-based bioprinting with hybrid GelMA-MeHA bioink was attempted which has not been extensively studied elsewhere.

5.3 The Way Forward

5.3.1 3D Bioprinting with Specialized Cell Types

The primary aim behind the use of Hyaluronic acid as a component of the bioprinted scaffold was to attain significant advantages due to the unique value proposition of HA as a biomaterial. Its ability to interact with cells through receptors like CD44 and RHAMM would allow the cells to behave in a way that is more similar to *In vivo* conditions. Therefore, through using HA within a scaffold it would be possible to study the behavior of specialized cell types such as neural and

cardiac cell types. The abundance of HA in the neural tissues makes it an exciting prospect for studying more delicate cell types like neurons. It would be an interesting study to observe and monitor the behavior of primary neurons within the HA scaffolds and compare them with other biomaterials-based matrices. It can be hypothesized that the MeHA scaffold would exhibit better proliferation and phenotype expression of these special cell types compared to other biomaterials. qPCR tests can be carried out to specifically identify the influence of MeHA on the cell and its phenotype.

Therefore, there is an immense scope of work with the use of MeHA and GelMA as a hybrid bioink to study specialized cell types and understanding the influence of scaffold microenvironments on their behavior.

5.3.2 Optimization of DLP-SLA Bioprinting with GelMA-MeHA Bioink

DLP-SLA-based bioprinting has not been explored in-depth but it has high potential because of its utility. The non-contact printing process, along with the utilization of visible light crosslinking makes it a far safer process for the use of cells compared to any other methods that use lasers, UV-radiation, or thermal and shear stress driven deposition. Moreover, the use of off-the-shelf components makes it cost-effective and easy to implement. Besides, it would enable the easiest translation of medical imaging into 3D bioprintable templates in the future. The work conducted in this thesis, lays out a strong foundation for DLP-SLA-based 3D bioprinting with GelMA-HA hybrid bioink. Therefore, in the future, there needs to be further optimization of the process. The hybrid bioink has shown to be compatible with the printing process but further optimization is required to scale its usage.

Optimization is required in the following aspects:

1) An optimum concentration and proportion of GelMA and MeHA used for printing. Determining the optimum proportion and concentration would depend on the specific application. Hence, on a case by case basis, each different application needs to be evaluated and optimized. The relevant mechanical properties, biocompatibility, biological functionality, and printing characteristics need to be considered.
2) An optimum distance of projection and crosslinking time. Again, on a case-by-case basis, an optimum projection distance and crosslinking time needs to be identified so that any concerns with under or over-crosslinking can be avoided. It can be achieved through a study of the gelation characteristic of the hybrid bioink.

Alongside the aforementioned parameters, there needs to be consistent efforts so that enhanced printing quality can be achieved and large-scale scaffolds can be printed.

5.3.3 Thermal *in-situ* Crosslinking and *in-vivo* Implant

The dual crosslinkability established through this thesis is unique. To the best of knowledge, this has not been implemented with 3D bioprinting with MeHA. Therefore, this trait of the dual-crosslinkable MeHA can open interesting avenues of research. The wound healing and inflammation-reducing capabilities of HA are well-known and utilized in the healthcare and cosmetic industry. Therefore, if the dual-crosslinkability is explored, then MeHA can be utilized as a wound healing and inflammation-reducing graft that can be crosslinked *in-situ*. As *in-situ* surgical options become increasingly more popular in the coming days, bioactive functionalized materials like MeHA would be indispensable.

Bibliography

[1] U.S. Department of Health & Human Services, National Data - OPTN, (2019).

[2] J.P. Vacanti, R. Langer, Tissue engineering: The design and fabrication of living replacement devices for surgical reconstruction and transplantation, Lancet. 354 (1999) 32–34. doi:10.1016/s0140-6736(99)90247-7.

[3] S. Baiguera, P. Jungebluth, A. Burns, C. Mavilia, J. Haag, P. De Coppi, P. Macchiarini, Tissue engineered human tracheas for in vivo implantation, Biomaterials. 31 (2010) 8931–8938. doi:10.1016/j.biomaterials.2010.08.005.

[4] T.H. Petersen, E.A. Calle, L. Zhao, E.J. Lee, L. Gui, M.B. Raredon, K. Gavrilov, T. Yi, Z.W. Zhuang, C. Breuer, E. Herzog, L.E. Niklason, Tissue-Engineered Lungs for in Vivo Implantation, Source Sci. New Ser. 329 (2010) 538–541. doi:10.1126/science.ll88308.

[5] A. Atala, S.B. Bauer, S. Soker, J.J. Yoo, A.B. Retik, Tissue-engineered autologous bladders for patients needing cystoplasty, Www.Thelancet.Com. 367 (2006). doi:10.1016/S0140.

[6] Z. Wang, R. Samanipour, K.I. Koo, K. Kim, Development and Investigation of a Sweetness Sensor for Sugars -Effect of Lipids-, Sensors Mater. 27 (2015) 1. doi:10.18494/SAM.2015.1086.

[7] J. Saji Joseph, S. Tebogo Malindisa, M. Ntwasa, Two-Dimensional (2D) and Three-Dimensional (3D) Cell Culturing in Drug Discovery, in: Cell Cult., IntechOpen, 2019. doi:10.5772/intechopen.81552.

[8] B. Subramanian, D. Rudym, C. Cannizzaro, R. Perrone, J. Zhou, D.L. Kaplan, Tissue-Engineered Three-Dimensional In Vitro Models for Normal and Diseased Kidney, Tissue Eng. Part A. 16 (2010) 2821–2831. doi:10.1089/ten.tea.2009.0595.

[9] T.M. DesRochers, E. Palma, D.L. Kaplan, Tissue-engineered kidney disease models, Adv.

Drug Deliv. Rev. 69–70 (2014) 67–80. doi:10.1016/j.addr.2013.12.002.

[10] M.E. Bregenzer, E.N. Horst, P. Mehta, C.M. Novak, S. Raghavan, C.S. Snyder, G. Mehta, Integrated cancer tissue engineering models for precision medicine, PLoS One. 14 (2019) e0216564. doi:10.1371/journal.pone.0216564.

[11] R. Bhowmick, T. Derakhshan, Y. Liang, J. Ritchey, L. Liu, H. Gappa-Fahlenkamp, A Three-Dimensional Human Tissue-Engineered Lung Model to Study Influenza A Infection, Tissue Eng. - Part A. 24 (2018) 1468–1480. doi:10.1089/ten.tea.2017.0449.

[12] Y. Liu, H. Luo, X. Wang, A. Takemura, Y.R. Fang, Y. Jin, F. Suwa, In Vitro Construction of Scaffold-Free Bilayered Tissue-Engineered Skin Containing Capillary Networks, Biomed Res. Int. 2013 (2013) 1–8. doi:10.1155/2013/561410.

[13] P. Bajaj, R.M. Schweller, A. Khademhosseini, J.L. West, R. Bashir, 3D Biofabrication Strategies for Tissue Engineering and Regenerative Medicine, Annu. Rev. Biomed. Eng. (2014). doi:10.1146/annurev-bioeng-071813-105155.

[14] J. Groll, T. Boland, T. Blunk, J.A. Burdick, D.-W. Cho, P.D. Dalton, B. Derby, G. Forgacs, Q. Li, V.A. Mironov, L. Moroni, M. Nakamura, W. Shu, S. Takeuchi, G. Vozzi, T.B.F. Woodfield, T. Xu, J.J. Yoo, J. Malda, Biofabrication: reappraising the definition of an evolving field, Biofabrication. 8 (2016) 013001. doi:10.1088/1758-5090/8/1/013001.

[15] M. Nie, S. Takeuchi, Bottom-up biofabrication using microfluidic techniques, Biofabrication. 10 (2018) 044103. doi:10.1088/1758-5090/aadef9.

[16] F. Guillemot, V. Mironov, M. Nakamura, Bioprinting is coming of age: report from the International Conference on Bioprinting and Biofabrication in Bordeaux (3B’09), Biofabrication. 2 (2010) 010201. doi:10.1088/1758-5082/2/1/010201.

[17] P. Ambhorkar, Z. Wang, H. Ko, S. Lee, K.I. Koo, K. Kim, D.I.D. Cho, Nanowire-based

biosensors: From growth to applications, Micromachines. 9 (2018) 679. doi:10.3390/mi9120679.

[18] E. Hoch, G.E.M. Tovar, K. Borchers, Bioprinting of artificial blood vessels: current approaches towards a demanding goal, Eur. J. Cardio-Thoracic Surg. 46 (2014) 767–778. doi:10.1093/ejcts/ezu242.

[19] Y. Xu, Y. Hu, C. Liu, H. Yao, B. Liu, S. Mi, A Novel Strategy for Creating Tissue-Engineered Biomimetic Blood Vessels Using 3D Bioprinting Technology., Mater. (Basel, Switzerland). 11 (2018). doi:10.3390/ma11091581.

[20] Y.S. Zhang, A. Arneri, S. Bersini, S.R. Shin, K. Zhu, Z. Goli-Malekabadi, J. Aleman, C. Colosi, F. Busignani, V. Dell'Erba, C. Bishop, T. Shupe, D. Demarchi, M. Moretti, M. Rasponi, M.R. Dokmeci, A. Atala, A. Khademhosseini, Bioprinting 3D microfibrous scaffolds for engineering endothelialized myocardium and heart-on-a-chip, Biomaterials. 110 (2016) 45–59. doi:10.1016/j.biomaterials.2016.09.003.

[21] N. Noor, A. Shapira, R. Edri, I. Gal, L. Wertheim, T. Dvir, 3D Printing of Personalized Thick and Perfusable Cardiac Patches and Hearts, Adv. Sci. 6 (2019) 1900344. doi:10.1002/advs.201900344.

[22] J. Kundu, J.-H. Shim, J. Jang, S.-W. Kim, D.-W. Cho, An additive manufacturing-based PCL-alginate-chondrocyte bioprinted scaffold for cartilage tissue engineering, J. Tissue Eng. Regen. Med. 9 (2015) 1286–1297. doi:10.1002/term.1682.

[23] D. Nguyen, D.A. Hägg, A. Forsman, J. Ekholm, P. Nimkingratana, C. Brantsing, T. Kalogeropoulos, S. Zaunz, S. Concaro, M. Brittberg, A. Lindahl, P. Gatenholm, A. Enejder, S. Simonsson, Cartilage Tissue Engineering by the 3D Bioprinting of iPS Cells in a Nanocellulose/Alginate Bioink, Sci. Rep. 7 (2017) 658. doi:10.1038/s41598-017-00690-y.

[24] W.C. Yan, P. Davoodi, S. Vijayavenkataraman, Y. Tian, W.C. Ng, J.Y.H. Fuh, K.S. Robinson, C.H. Wang, 3D bioprinting of skin tissue: From pre-processing to final product evaluation, Adv. Drug Deliv. Rev. 132 (2018) 270–295. doi:10.1016/j.addr.2018.07.016.

[25] W. Li, X. Hu, S. Yang, S. Wang, C. Zhang, H. Wang, Y.Y. Cheng, Y. Wang, T. Liu, K. Song, A novel tissue-engineered 3D tumor model for anti-cancer drug discovery, Biofabrication. 11 (2018) 015004. doi:10.1088/1758-5090/aae270.

[26] M. Thomas, S.M. Willerth, 3-D Bioprinting of Neural Tissue for Applications in Cell Therapy and Drug Screening, Front. Bioeng. Biotechnol. 5 (2017) 69. doi:10.3389/fbioe.2017.00069.

[27] A.Y. Hsiao, T. Okitsu, H. Teramae, S. Takeuchi, 3D Tissue Formation of Unilocular Adipocytes in Hydrogel Microfibers, Adv. Healthc. Mater. 5 (2016) 548–556. doi:10.1002/adhm.201500673.

[28] L. Ouyang, R. Yao, S. Mao, X. Chen, J. Na, W. Sun, Three-dimensional bioprinting of embryonic stem cells directs highly uniform embryoid body formation, Biofabrication. 7 (2015) 044101. doi:10.1088/1758-5090/7/4/044101.

[29] R. Dai, Z. Wang, R. Samanipour, K. Koo, K. Kim, Adipose-Derived Stem Cells for Tissue Engineering and Regenerative Medicine Applications, Stem Cells Int. 2016 (2016) 1–19. doi:10.1155/2016/6737345.

[30] M. Radisic, L. Yang, J. Boublik, R.J. Cohen, R. Langer, L.E. Freed, G. Vunjak-Novakovic, Medium perfusion enables engineering of compact and contractile cardiac tissue, Am. J. Physiol. Circ. Physiol. 286 (2004) H507–H516. doi:10.1152/ajpheart.00171.2003.

[31] P. Ambhorkar, R.H. Rakin, Z. Wang, H. Kumar, K. Kim, Biofabrication strategies for engineering heterogeneous artificial tissues, Addit. Manuf. 36 (2020) 101459.

doi:10.1016/j.addma.2020.101459.

[32] C. Mandrycky, Z. Wang, K. Kim, D.-H. Kim, 3D bioprinting for engineering complex tissues, Biotechnol. Adv. 34 (2016) 422–434. doi:10.1016/j.biotechadv.2015.12.011.

[33] Y. Morimoto, A.Y. Hsiao, S. Takeuchi, Point-, line-, and plane-shaped cellular constructs for 3D tissue assembly, Adv. Drug Deliv. Rev. 95 (2015) 29–39. doi:10.1016/j.addr.2015.09.003.

[34] J. Schöneberg, F. De Lorenzi, B. Theek, A. Blaeser, D. Rommel, A.J.C. Kuehne, F. Kießling, H. Fischer, Engineering biofunctional in vitro vessel models using a multilayer bioprinting technique, Sci. Rep. 8 (2018) 10430. doi:10.1038/s41598-018-28715-0.

[35] S. Azizi Machekposhti, S. Mohaved, R.J. Narayan, Inkjet dispensing technologies: recent advances for novel drug discovery, Expert Opin. Drug Discov. 14 (2019) 101–113. doi:10.1080/17460441.2019.1567489.

[36] T. Xu, W. Zhao, J.M. Zhu, M.Z. Albanna, J.J. Yoo, A. Atala, Complex heterogeneous tissue constructs containing multiple cell types prepared by inkjet printing technology, Biomaterials. 34 (2013) 130–139. doi:10.1016/j.biomaterials.2012.09.035.

[37] A. Bsoul, S. Pan, E. Cretu, B. Stoeber, K. Walus, Design, microfabrication, and characterization of a moulded PDMS/SU-8 inkjet dispenser for a Lab-on-a-Printer platform technology with disposable microfluidic chip, Lab Chip. 16 (2016) 3351–3361. doi:10.1039/C6LC00636A.

[38] S. Sakai, K. Ueda, E. Gantumur, M. Taya, M. Nakamura, Drop-On-Drop Multimaterial 3D Bioprinting Realized by Peroxidase-Mediated Cross-Linking, Macromol. Rapid Commun. 39 (2018) 1700534. doi:10.1002/marc.201700534.

[39] S. Yoon, J.A. Park, H.-R. Lee, W.H. Yoon, D.S. Hwang, S. Jung, Inkjet-Spray Hybrid

Printing for 3D Freeform Fabrication of Multilayered Hydrogel Structures, Adv. Healthc. Mater. 7 (2018) 1800050. doi:10.1002/adhm.201800050.

[40] J.K. Placone, A.J. Engler, Recent Advances in Extrusion-Based 3D Printing for Biomedical Applications, Adv. Healthc. Mater. 7 (2018) 1701161. doi:10.1002/adhm.201701161.

[41] C. Colosi, S.R. Shin, V. Manoharan, S. Massa, M. Costantini, A. Barbetta, M.R. Dokmeci, M. Dentini, A. Khademhosseini, Microfluidic Bioprinting of Heterogeneous 3D Tissue Constructs Using Low-Viscosity Bioink, Adv. Mater. 28 (2016) 677–684. doi:10.1002/adma.201503310.

[42] M. Costantini, S. Testa, P. Mozetic, A. Barbetta, C. Fuoco, E. Fornetti, F. Tamiro, S. Bernardini, J. Jaroszewicz, W. Święszkowski, M. Trombetta, L. Castagnoli, D. Seliktar, P. Garstecki, G. Cesareni, S. Cannata, A. Rainer, C. Gargioli, Microfluidic-enhanced 3D bioprinting of aligned myoblast-laden hydrogels leads to functionally organized myofibers in vitro and in vivo, Biomaterials. 131 (2017) 98–110. doi:10.1016/J.BIOMATERIALS.2017.03.026.

[43] M. Costantini, C. Colosi, W. Święszkowski, A. Barbetta, Co-axial wet-spinning in 3D bioprinting: State of the art and future perspective of microfluidic integration, Biofabrication. 11 (2019) 012001. doi:10.1088/1758-5090/aae605.

[44] W. Liu, Z. Zhong, N. Hu, Y. Zhou, L. Maggio, A.K. Miri, A. Fragasso, X. Jin, A. Khademhosseini, Y.S. Zhang, Coaxial extrusion bioprinting of 3D microfibrous constructs with cell-favorable gelatin methacryloyl microenvironments, Biofabrication. 10 (2018) 024102. doi:10.1088/1758-5090/aa9d44.

[45] L. Ouyang, C.B. Highley, W. Sun, J.A. Burdick, A Generalizable Strategy for the 3D Bioprinting of Hydrogels from Nonviscous Photo-crosslinkable Inks, Adv. Mater. 29

(2017) 1604983. doi:10.1002/adma.201604983.

[46] D. Kang, G. Ahn, D. Kim, H.-W. Kang, S. Yun, W.-S. Yun, J.-H. Shim, S. Jin, Pre-set extrusion bioprinting for multiscale heterogeneous tissue structure fabrication, Biofabrication. 10 (2018) 035008. doi:10.1088/1758-5090/aac70b.

[47] H. Yuk, X. Zhao, A New 3D Printing Strategy by Harnessing Deformation, Instability, and Fracture of Viscoelastic Inks, Adv. Mater. 30 (2018) 1704028. doi:10.1002/adma.201704028.

[48] P. Zhuang, A.X. Sun, J. An, C.K. Chua, S.Y. Chew, 3D neural tissue models: From spheroids to bioprinting, Biomaterials. 154 (2018) 113–133. doi:10.1016/j.biomaterials.2017.10.002.

[49] G. Potjewyd, S. Moxon, T. Wang, M. Domingos, N.M. Hooper, Tissue Engineering 3D Neurovascular Units: A Biomaterials and Bioprinting Perspective, Trends Biotechnol. 36 (2018) 457–472. doi:10.1016/j.tibtech.2018.01.003.

[50] T.J. Esworthy, S. Miao, S.-J. Lee, X. Zhou, H. Cui, Y.Y. Zuo, L.G. Zhang, Advanced 4D-bioprinting technologies for brain tissue modeling and study, Int. J. Smart Nano Mater. 10 (2019) 177–204. doi:10.1080/19475411.2019.1631899.

[51] R. Lozano, L. Stevens, B.C. Thompson, K.J. Gilmore, R. Gorkin, E.M. Stewart, M. in het Panhuis, M. Romero-Ortega, G.G. Wallace, 3D printing of layered brain-like structures using peptide modified gellan gum substrates, Biomaterials. 67 (2015) 264–273. doi:10.1016/j.biomaterials.2015.07.022.

[52] M.S. Ozturk, V.K. Lee, H. Zou, R.H. Friedel, G. Dai, X. Intes, High Resolution Tomographic Analysis of in vitro 3D Glioblastoma Tumor Model under Long-Term Drug Treatment, BioRxiv. 6 (2019) eaay7513. doi:10.1101/684019.

[53] K. Zhu, S.R. Shin, T. van Kempen, Y. Li, V. Ponraj, A. Nasajpour, S. Mandla, N. Hu, X. Liu, J. Leijten, Gold nanocomposite bioink for printing 3D cardiac constructs, Adv. Funct. Mater. 27 (2017) 1605352.

[54] S.R. Shin, C. Zihlmann, M. Akbari, P. Assawes, L. Cheung, K. Zhang, V. Manoharan, Y.S. Zhang, M. Yüksekkaya, K. Wan, M. Nikkhah, M.R. Dokmeci, X.S. Tang, A. Khademhosseini, Reduced Graphene Oxide-GelMA Hybrid Hydrogels as Scaffolds for Cardiac Tissue Engineering, Small. 12 (2016) 3677–3689. doi:10.1002/smll.201600178.

[55] N. Noor, A. Shapira, R. Edri, I. Gal, L. Wertheim, T. Dvir, 3D Printing of Personalized Thick and Perfusable Cardiac Patches and Hearts, Adv. Sci. (2019) 1900344. doi:10.1002/advs.201900344.

[56] T.J. Hinton, Q. Jallerat, R.N. Palchesko, J.H. Park, M.S. Grodzicki, H.J. Shue, M.H. Ramadan, A.R. Hudson, A.W. Feinberg, Three-dimensional printing of complex biological structures by freeform reversible embedding of suspended hydrogels, Sci. Adv. 1 (2015) e1500758. doi:10.1126/sciadv.1500758.

[57] A. Lee, A.R. Hudson, D.J. Shiwarski, J.W. Tashman, T.J. Hinton, S. Yerneni, J.M. Bliley, P.G. Campbell, A.W. Feinberg, 3D bioprinting of collagen to rebuild components of the human heart, Science (80-.). 365 (2019) 482–487. doi:10.1126/science.aav9051.

[58] H. Kumar, K. Kim, Stereolithography 3D Bioprinting, in: Methods Mol. Biol., NLM (Medline), 2020: pp. 93–108. doi:10.1007/978-1-0716-0520-2_6.

[59] R. Gauvin, Y.-C.C. Chen, J.W. Lee, P. Soman, P. Zorlutuna, J.W. Nichol, H. Bae, S. Chen, A. Khademhosseini, Microfabrication of complex porous tissue engineering scaffolds using 3D projection stereolithography, Biomaterials. 33 (2012) 3824–3834. doi:10.1016/j.biomaterials.2012.01.048.

[60] Z. Wang, R. Abdulla, B. Parker, R. Samanipour, S. Ghosh, K. Kim, A simple and high-resolution stereolithography-based 3D bioprinting system using visible light crosslinkable bioinks, Biofabrication. In press (2016).

[61] K.C. Hribar, K. Meggs, J. Liu, W. Zhu, X. Qu, S. Chen, Three-dimensional direct cell patterning in collagen hydrogels with near-infrared femtosecond laser, Sci. Rep. 5 (2015) 17203. doi:10.1038/srep17203.

[62] Z. Wang, X. Jin, R. Dai, J.F. Holzman, K. Kim, An ultrafast hydrogel photocrosslinking method for direct laser bioprinting, RSC Adv. 6 (2016) 21099–21104. doi:10.1039/C5RA24910D.

[63] R. Raman, B. Bhaduri, M. Mir, A. Shkumatov, M.K. Lee, G. Popescu, H. Kong, R. Bashir, High-Resolution Projection Microstereolithography for Patterning of Neovasculature, Adv. Healthc. Mater. 5 (2016) 610–619. doi:10.1002/adhm.201500721.

[64] A.K. Miri, D. Nieto, L. Iglesias, H. Goodarzi Hosseinabadi, S. Maharjan, G.U. Ruiz-Esparza, P. Khoshakhlagh, A. Manbachi, M.R. Dokmeci, S. Chen, S.R. Shin, Y.S. Zhang, A. Khademhosseini, Microfluidics-Enabled Multimaterial Maskless Stereolithographic Bioprinting, Adv. Mater. 30 (2018) 1800242. doi:10.1002/adma.201800242.

[65] Z. Wang, H. Kumar, Z. Tian, X. Jin, J.F. Holzman, F. Menard, K. Kim, Visible Light Photoinitiation of Cell-Adhesive Gelatin Methacryloyl Hydrogels for Stereolithography 3D Bioprinting, (2018). doi:10.1021/acsami.8b06607.

[66] X. Ma, C. Yu, P. Wang, W. Xu, X. Wan, C.S.E. Lai, J. Liu, A. Koroleva-Maharajh, S. Chen, Rapid 3D bioprinting of decellularized extracellular matrix with regionally varied mechanical properties and biomimetic microarchitecture, Biomaterials. 185 (2018) 310–321. doi:10.1016/j.biomaterials.2018.09.026.

[67] C. Yu, S. You, W. Zhu, B. Sun, S. Chen, DMD-based rapid 3D bioprinting for precision tissue engineering and regenerative medicine, in: B.L. Lee, J. Ehmke (Eds.), Emerg. Digit. Micromirror Device Based Syst. Appl. XII, SPIE, 2020: p. 4. doi:10.1117/12.2550340.

[68] M. Ali, P.R. Anil Kumar, J.J. Yoo, F. Zahran, A. Atala, S.J. Lee, A Photo-Crosslinkable Kidney ECM-Derived Bioink Accelerates Renal Tissue Formation, Adv. Healthc. Mater. 8 (2019) 1800992. doi:10.1002/adhm.201800992.

[69] P.N. Bernal, P. Delrot, D. Loterie, Y. Li, J. Malda, C. Moser, R. Levato, Volumetric Bioprinting of Complex Living-Tissue Constructs within Seconds, Adv. Mater. 31 (2019) 1904209. doi:10.1002/adma.201904209.

[70] L. Gasperini, J.F. Mano, R.L. Reis, Natural polymers for the microencapsulation of cells, J. R. Soc. Interface. 11 (2014) 20140817. doi:10.1098/rsif.2014.0817.

[71] S. Sakai, K. Hirose, K. Taguchi, Y. Ogushi, K. Kawakami, An injectable, in situ enzymatically gellable, gelatin derivative for drug delivery and tissue engineering, Biomaterials. 30 (2009) 3371–3377. doi:10.1016/j.biomaterials.2009.03.030.

[72] J.A. Benton, C.A. DeForest, V. Vivekanandan, K.S. Anseth, Photocrosslinking of Gelatin Macromers to Synthesize Porous Hydrogels That Promote Valvular Interstitial Cell Function, Tissue Eng. Part A. 15 (2009) 3221–3230. doi:10.1089/ten.tea.2008.0545.

[73] X. Wang, Y. Yan, Y. Pan, Z. Xiong, H. Liu, J. Cheng, F. Liu, F. Lin, R. Wu, R. Zhang, Q. Lu, Generation of three-dimensional hepatocyte/gelatin structures with rapid prototyping system, Tissue Eng. 12 (2006) 83–90. doi:10.1089/ten.2006.12.83.

[74] T. Boland, X. Tao, B.J. Damon, B. Manley, P. Kesari, S. Jalota, S. Bhaduri, Drop-on-demand printing of cells and materials for designer tissue constructs, Mater. Sci. Eng. C. 27 (2007) 372–376. doi:10.1016/j.msec.2006.05.047.

[75] N.A. Raof, N.R. Schiele, Y. Xie, D.B. Chrisey, D.T. Corr, The maintenance of pluripotency following laser direct-write of mouse embryonic stem cells, Biomaterials. 32 (2011) 1802–1808. doi:10.1016/j.biomaterials.2010.11.015.

[76] J.W. Nichol, S.T. Koshy, H. Bae, C.M. Hwang, S. Yamanlar, A. Khademhosseini, Cell-laden microengineered gelatin methacrylate hydrogels, Biomaterials. 31 (2010) 5536–5544. doi:10.1016/j.biomaterials.2010.03.064.

[77] A.R. Spencer, E. Shirzaei Sani, J.R. Soucy, C.C. Corbet, A. Primbetova, R.A. Koppes, N. Annabi, Bioprinting of a Cell-Laden Conductive Hydrogel Composite, ACS Appl. Mater. Interfaces. 11 (2019) 30518–30533. doi:10.1021/acsami.9b07353.

[78] Z. Wang, R. Abdulla, B. Parker, R. Samanipour, S. Ghosh, K. Kim, A simple and high-resolution stereolithography-based 3D bioprinting system using visible light crosslinkable bioinks, Biofabrication. 7 (2015) 045009. doi:10.1088/1758-5090/7/4/045009.

[79] R. Gauvin, Y.-C. Chen, J.W. Lee, P. Soman, P. Zorlutuna, J.W. Nichol, H. Bae, S. Chen, A. Khademhosseini, Microfabrication of complex porous tissue engineering scaffolds using 3D projection stereolithography, Biomaterials. 33 (2012) 3824–3834. doi:10.1016/j.biomaterials.2012.01.048.

[80] K. Sakthivel, H. Kumar, M.G.A. Mohamed, B. Talebjedi, J. Shim, H. Najjaran, M. Hoorfar, K. Kim, High Throughput Screening of Cell Mechanical Response Using a Stretchable 3D Cellular Microarray Platform, Small. 16 (2020) 2000941. doi:10.1002/smll.202000941.

[81] M. Xie, Q. Gao, H. Zhao, J. Nie, Z. Fu, H. Wang, L. Chen, L. Shao, J. Fu, Z. Chen, Y. He, Electro-Assisted Bioprinting of Low-Concentration GelMA Microdroplets, Small. 15 (2019) 1804216. doi:10.1002/smll.201804216.

[82] F. Ruther, T. Distler, A.R. Boccaccini, R. Detsch, Biofabrication of vessel-like structures

with alginate di-aldehyde—gelatin (ADA-GEL) bioink, J. Mater. Sci. Mater. Med. 30 (2019) 1–14. doi:10.1007/s10856-018-6205-7.

[83] K.K. Lai, R. Renneberg, W.C. Mak, High efficiency single-step biomaterial-based microparticle fabrication via template-directed supramolecular coordination chemistry, Green Chem. 18 (2016) 1715–1723. doi:10.1039/c5gc02424b.

[84] M. Hospodiuk, M. Dey, D. Sosnoski, I.T. Ozbolat, The bioink: A comprehensive review on bioprintable materials, Biotechnol. Adv. 35 (2017) 217–239. doi:10.1016/j.biotechadv.2016.12.006.

[85] M. Hospodiuk, M. Dey, D. Sosnoski, I.T. Ozbolat, The bioink: A comprehensive review on bioprintable materials, Biotechnol. Adv. 35 (2017) 217–239. doi:https://doi.org/10.1016/j.biotechadv.2016.12.006.

[86] J.A. Rowley, G. Madlambayan, D.J. Mooney, Alginate hydrogels as synthetic extracellular matrix materials, Biomaterials. 20 (1999) 45–53. doi:10.1016/S0142-9612(98)00107-0.

[87] K.Y. Lee, D.J. Mooney, Alginate: Properties and biomedical applications, Prog. Polym. Sci. 37 (2012) 106–126. doi:10.1016/j.progpolymsci.2011.06.003.

[88] K. Markstedt, A. Mantas, I. Tournier, H. Martínez Ávila, D. Hägg, P. Gatenholm, 3D Bioprinting Human Chondrocytes with Nanocellulose–Alginate Bioink for Cartilage Tissue Engineering Applications, Biomacromolecules. 16 (2015) 1489–1496. doi:10.1021/acs.biomac.5b00188.

[89] H. Gudapati, M. Dey, I. Ozbolat, A comprehensive review on droplet-based bioprinting: Past, present and future, Biomaterials. 102 (2016) 20–42. doi:10.1016/j.biomaterials.2016.06.012.

[90] H. Gudapati, J. Yan, Y. Huang, D.B. Chrisey, Alginate gelation-induced cell death during

laser-assisted cell printing, Biofabrication. 6 (2014) 035022. doi:10.1088/1758-5082/6/3/035022.

[91] J. Yan, Y. Huang, D.B. Chrisey, Laser-assisted printing of alginate long tubes and annular constructs, Biofabrication. 5 (2013) 015002. doi:10.1088/1758-5082/5/1/015002.

[92] A.M. Ferreira, P. Gentile, V. Chiono, G. Ciardelli, Collagen for bone tissue regeneration, Acta Biomater. 8 (2012) 3191–3200. doi:10.1016/j.actbio.2012.06.014.

[93] K.K. Moncal, V. Ozbolat, P. Datta, D.N. Heo, I.T. Ozbolat, Thermally-controlled extrusion-based bioprinting of collagen, J. Mater. Sci. Mater. Med. 30 (2019) 1–14. doi:10.1007/s10856-019-6258-2.

[94] S. Michael, H. Sorg, C.T. Peck, L. Koch, A. Deiwick, B. Chichkov, P.M. Vogt, K. Reimers, Tissue Engineered Skin Substitutes Created by Laser-Assisted Bioprinting Form Skin-Like Structures in the Dorsal Skin Fold Chamber in Mice, PLoS One. 8 (2013) e57741. doi:10.1371/journal.pone.0057741.

[95] N.E. Fedorovich, J.R. De Wijn, A.J. Verbout, J. Alblas, W.J.A. Dhert, Three-dimensional fiber deposition of cell-laden, viable, patterned constructs for bone tissue printing, Tissue Eng. - Part A. 14 (2008) 127–133. doi:10.1089/ten.a.2007.0158.

[96] C.M. Livoti, J.R. Morgan, Self-assembly and tissue fusion of toroid-shaped minimal building units, Tissue Eng. - Part A. 16 (2010) 2051–2061. doi:10.1089/ten.tea.2009.0607.

[97] D.F.D. Campos, A. Blaeser, A. Korsten, S. Neuss, J. Jäkel, M. Vogt, H. Fischer, The stiffness and structure of three-dimensional printed hydrogels direct the differentiation of mesenchymal stromal cells toward adipogenic and osteogenic lineages, Tissue Eng. - Part A. 21 (2015) 740–756. doi:10.1089/ten.tea.2014.0231.

[98] T. Xu, J. Jin, C. Gregory, J.J. Hickman, T. Boland, Inkjet printing of viable mammalian

cells, Biomaterials. 26 (2005) 93–99. doi:10.1016/j.biomaterials.2004.04.011.

[99] L. Koch, S. Kuhn, H. Sorg, M. Gruene, S. Schlie, R. Gaebel, B. Polchow, K. Reimers, S. Stoelting, N. Ma, P.M. Vogt, G. Steinhoff, B. Chichkov, Laser printing of skin cells and human stem cells, Tissue Eng. - Part C Methods. 16 (2010) 847–854. doi:10.1089/ten.tec.2009.0397.

[100] R.M. Olabisi, Cell microencapsulation with synthetic polymers, J. Biomed. Mater. Res. Part A. 103 (2015) 846–859. doi:10.1002/jbm.a.35205.

[101] M. Mesa, L. Sierra, J. Patarin, J.L. Guth, Morphology and porosity characteristics control of SBA-16 mesoporous silica. Effect of the triblock surfactant Pluronic F127 degradation during the synthesis, Solid State Sci. 7 (2005) 990–997. doi:10.1016/j.solidstatesciences.2005.04.006.

[102] C.Y. Gong, S. Shi, P.W. Dong, X.L. Zheng, S.Z. Fu, G. Guo, J.L. Yang, Y.Q. Wei, Z.Y. Qian, In vitro drug release behavior from a novel thermosensitive composite hydrogel based on Pluronic f127 and poly(ethylene glycol)-poly(ε-caprolactone)-poly(ethylene glycol) copolymer, BMC Biotechnol. 9 (2009) 8. doi:10.1186/1472-6750-9-8.

[103] M.K. Johnson, F. Coley, A. Raj, E.H. Adelson, Microgeometry Capture using an Elastomeric Sensor, ACM Trans. Graph. 30 (2011) 1–8. doi:10.1145/2010324.1964941.

[104] L.E. Bertassoni, M. Cecconi, V. Manoharan, M. Nikkhah, J. Hjortnaes, A.L. Cristino, G. Barabaschi, D. Demarchi, M.R. Dokmeci, Y. Yang, A. Khademhosseini, Hydrogel bioprinted microchannel networks for vascularization of tissue engineering constructs, Lab Chip. 14 (2014) 2202. doi:10.1039/c4lc00030g.

[105] L.A. Hockaday, K.H. Kang, N.W. Colangelo, P.Y.C. Cheung, B. Duan, E. Malone, J. Wu, L.N. Girardi, L.J. Bonassar, H. Lipson, C.C. Chu, J.T. Butcher, Rapid 3D printing of

anatomically accurate and mechanically heterogeneous aortic valve hydrogel scaffolds, Biofabrication. 4 (2012) 035005. doi:10.1088/1758-5082/4/3/035005.

[106] S. Wüst, M.E. Godla, R. Müller, S. Hofmann, Tunable hydrogel composite with two-step processing in combination with innovative hardware upgrade for cell-based three-dimensional bioprinting, Acta Biomater. 10 (2014) 630–640. doi:10.1016/j.actbio.2013.10.016.

[107] X. Cui, K. Breitenkamp, M.G. Finn, M. Lotz, D.D. D'Lima, Direct human cartilage repair using three-dimensional bioprinting technology, Tissue Eng. - Part A. 18 (2012) 1304–1312. doi:10.1089/ten.tea.2011.0543.

[108] X. Cui, K. Breitenkamp, M. Lotz, D. D'Lima, Synergistic action of fibroblast growth factor-2 and transforming growth factor-beta1 enhances bioprinted human neocartilage formation, Biotechnol. Bioeng. 109 (2012) 2357–2368. doi:10.1002/bit.24488.

[109] B. Dhariwala, E. Hunt, T. Boland, Rapid prototyping of tissue-engineering constructs, using photopolymerizable hydrogels and stereolithography, Tissue Eng. 10 (2004) 1316–1322. doi:10.1089/ten.2004.10.1316.

[110] K.A. Smeds, A. Pfister-Serres, D.L. Hatchell &, M.W. Grinstaff, SYNTHESIS OF A NOVEL POLYSACCHARIDE HYDROGEL, J. Macromol. Sci. Appl. Chem. 36 (1999) 981–989. doi:10.1080/10601329908951194.

[111] G.D. W, Hyaluronic acid as a (bio)ink for extrusion-based 3D printing, (2020). doi:10.1088/1758-5090/ab8752.

[112] M.A. Selyanin, P.Y. Boykov, V.N. Khabarov, F. Polyak, The History of Hyaluronic Acid Discovery, Foundational Research and Initial Use, in: Hyaluronic Acid, John Wiley & Sons, Ltd, Chichester, UK, 2015: pp. 1–8. doi:10.1002/9781118695920.ch1.

[113] J.E. Rayahin, J.S. Buhrman, Y. Zhang, T.J. Koh, R.A. Gemeinhart, High and Low Molecular Weight Hyaluronic Acid Differentially Influence Macrophage Activation, ACS Biomater. Sci. Eng. 1 (2015) 481–493. doi:10.1021/acsbiomaterials.5b00181.

[114] A. Stellavato, V. Vassallo, A. La Gatta, A.V.A. Pirozzi, M. De Rosa, G. Balato, A. D'Addona, V. Tirino, C. Ruosi, C. Schiraldi, Novel Hybrid Gels Made of High and Low Molecular Weight Hyaluronic Acid Induce Proliferation and Reduce Inflammation in an Osteoarthritis In Vitro Model Based on Human Synoviocytes and Chondrocytes, Biomed Res. Int. 2019 (2019) 1–13. doi:10.1155/2019/4328219.

[115] M.N. Collins, C. Birkinshaw, Hyaluronic acid based scaffolds for tissue engineering-A review, Carbohydr. Polym. 92 (2013) 1262–1279. doi:10.1016/j.carbpol.2012.10.028.

[116] C. Loebel, C.B. Rodell, M.H. Chen, J.A. Burdick, Shear-thinning and self-healing hydrogels as injectable therapeutics and for 3D-printing, Nat. Protoc. 12 (2017) 1521–1541. doi:10.1038/nprot.2017.053.

[117] M.T. Poldervaart, B. Goversen, M. de Ruijter, A. Abbadessa, F.P.W. Melchels, F.C. Öner, W.J.A. Dhert, T. Vermonden, J. Alblas, 3D bioprinting of methacrylated hyaluronic acid (MeHA) hydrogel with intrinsic osteogenicity, PLoS One. 12 (2017) e0177628. doi:10.1371/journal.pone.0177628.

[118] V.H.M. Mouser, R. Levato, A. Mensinga, W.J.A. Dhert, D. Gawlitta, J. Malda, Bio-ink development for three-dimensional bioprinting of hetero-cellular cartilage constructs, Connect. Tissue Res. 61 (2020) 137–151. doi:10.1080/03008207.2018.1553960.

[119] D. van der Valk, C. van der Ven, M. Blaser, J. Grolman, P.-J. Wu, O. Fenton, L. Lee, M. Tibbitt, J. Andresen, J. Wen, A. Ha, F. Buffolo, A. van Mil, C. Bouten, S. Body, D. Mooney, J. Sluijter, M. Aikawa, J. Hjortnaes, R. Langer, E. Aikawa, Engineering a 3D-Bioprinted

Model of Human Heart Valve Disease Using Nanoindentation-Based Biomechanics, Nanomaterials. 8 (2018) 296. doi:10.3390/nano8050296.

[120] A. Wenz, K. Borchers, G.E.M. Tovar, P.J. Kluger, Bone matrix production in hydroxyapatite-modified hydrogels suitable for bone bioprinting, Biofabrication. 9 (2017) 044103. doi:10.1088/1758-5090/aa91ec.

[121] A. Skardal, J. Zhang, L. McCoard, X. Xu, S. Oottamasathien, G.D. Prestwich, Photocrosslinkable hyaluronan-gelatin hydrogels for two-step bioprinting, Tissue Eng. - Part A. 16 (2010) 2675–2685. doi:10.1089/ten.tea.2009.0798.

[122] G. Camci-Unal, D. Cuttica, N. Annabi, D. Demarchi, A. Khademhosseini, Synthesis and characterization of hybrid hyaluronic acid-gelatin hydrogels, Biomacromolecules. 14 (2013) 1085–1092. doi:10.1021/bm3019856.

[123] C.D. O'Connell, C. Di Bella, F. Thompson, C. Augustine, S. Beirne, R. Cornock, C.J. Richards, J. Chung, S. Gambhir, Z. Yue, J. Bourke, B. Zhang, A. Taylor, A. Quigley, R. Kapsa, P. Choong, G.G. Wallace, Development of the Biopen: a handheld device for surgical printing of adipose stem cells at a chondral wound site, Biofabrication. 8 (2016) 015019. doi:10.1088/1758-5090/8/1/015019.

[124] C.C. Clark, J. Aleman, L. Mutkus, A. Skardal, A mechanically robust thixotropic collagen and hyaluronic acid bioink supplemented with gelatin nanoparticles, Bioprinting. 16 (2019) e00058. doi:10.1016/j.bprint.2019.e00058.

[125] N. Law, B. Doney, H. Glover, Y. Qin, Z.M. Aman, T.B. Sercombe, L.J. Liew, R.J. Dilley, B.J. Doyle, Characterisation of hyaluronic acid methylcellulose hydrogels for 3D bioprinting, J. Mech. Behav. Biomed. Mater. 77 (2018) 389–399. doi:10.1016/J.JMBBM.2017.09.031.

[126] A. Rajaram, D.J. Schreyer, D.X.B. Chen, Use of the polycation polyethyleneimine to improve the physical properties of alginate-hyaluronic acid hydrogel during fabrication of tissue repair scaffolds, J. Biomater. Sci. Polym. Ed. 26 (2015) 433–445. doi:10.1080/09205063.2015.1016383.

[127] M. Müller, J. Becher, M. Schnabelrauch, M. Zenobi-Wong, Nanostructured Pluronic hydrogels as bioinks for 3D bioprinting, Biofabrication. 7 (2015) 035006. doi:10.1088/1758-5090/7/3/035006.

[128] A. Skardal, J. Zhang, G.D. Prestwich, Bioprinting vessel-like constructs using hyaluronan hydrogels crosslinked with tetrahedral polyethylene glycol tetracrylates, Biomaterials. 31 (2010) 6173–6181. doi:10.1016/j.biomaterials.2010.04.045.

[129] M. Costantini, J. Idaszek, K. Szöke, J. Jaroszewicz, M. Dentini, A. Barbetta, J.E. Brinchmann, W. Święszkowski, 3D bioprinting of BM-MSCs-loaded ECM biomimetic hydrogels for in vitro neocartilage formation, Biofabrication. 8 (2016) 035002. doi:10.1088/1758-5090/8/3/035002.

[130] J.H. Shin, H.W. Kang, The Development of Gelatin-Based Bio-Ink for Use in 3D Hybrid Bioprinting, Int. J. Precis. Eng. Manuf. 19 (2018) 767–771. doi:10.1007/s12541-018-0092-1.

[131] J.B. Leach, K.A. Bivens, C.W. Patrick, C.E. Schmidt, Photocrosslinked hyaluronic acid hydrogels: Natural, biodegradable tissue engineering scaffolds, Biotechnol. Bioeng. 82 (2003) 578–589. doi:10.1002/bit.10605.

[132] S.A. Bencherif, A. Srinivasan, F. Horkay, J.O. Hollinger, K. Matyjaszewski, N.R. Washburn, Influence of the degree of methacrylation on hyaluronic acid hydrogels properties, Biomaterials. 29 (2008) 1739–1749. doi:10.1016/j.biomaterials.2007.11.047.

[133] Q. Li, D.A. Wang, J.H. Elisseeff, Heterogeneous-phase reaction of glycidyl methacrylate and chondroitin sulfate: Mechanism of ring-opening-transesterification competition, Macromolecules. 36 (2003) 2556–2562. doi:10.1021/ma021190w.

[134] J.A. Burdick, C. Chung, X. Jia, M.A. Randolph, R. Langer, Controlled degradation and mechanical behavior of photopolymerized hyaluronic acid networks, Biomacromolecules. 6 (2005) 386–391. doi:10.1021/bm049508a.

[135] M.H.M. Oudshoorn, R. Rissmann, J.A. Bouwstra, W.E. Hennink, Synthesis of methacrylated hyaluronic acid with tailored degree of substitution, Polymer (Guildf). 48 (2007) 1915–1920. doi:10.1016/j.polymer.2007.01.068.

[136] M.L. Oyen, Mechanical characterisation of hydrogel materials, Int. Mater. Rev. 59 (2014) 44–59. doi:10.1179/1743280413Y.0000000022.

[137] D. Tarus, L. Hamard, F. Caraguel, D. Wion, A. Szarpak-Jankowska, B. Van Der Sanden, R. Auzély-Velty, Design of Hyaluronic Acid Hydrogels to Promote Neurite Outgrowth in Three Dimensions, ACS Appl. Mater. Interfaces. 8 (2016) 25051–25059. doi:10.1021/acsami.6b06446.

[138] H. Kumar, K. Sakthivel, M.G.A. Mohamed, E. Boras, S.R. Shin, K. Kim, Designing Gelatin Methacryloyl (GelMA)-Based Bioinks for Visible Light Stereolithographic 3D Biofabrication, Macromol. Biosci. (2020) 2000317. doi:10.1002/mabi.202000317.

[139] T. Yeung, P.C. Georges, L.A. Flanagan, B. Marg, M. Ortiz, M. Funaki, N. Zahir, W. Ming, V. Weaver, P.A. Janmey, Effects of substrate stiffness on cell morphology, cytoskeletal structure, and adhesion, Cell Motil. Cytoskeleton. 60 (2005) 24–34. doi:10.1002/cm.20041.

[140] J. Shi, M.M.Q. Xing, W. Zhong, Development of Hydrogels and Biomimetic Regulators as Tissue Engineering Scaffolds, Membranes (Basel). 2 (2012) 70–90.

doi:10.3390/membranes2010070.

[141] M. Dadsetan, T.E. Hefferan, J.P. Szatkowski, P.K. Mishra, S.I. Macura, L. Lu, M.J. Yaszemski, Effect of hydrogel porosity on marrow stromal cell phenotypic expression, Biomaterials. 29 (2008) 2193–2202. doi:10.1016/j.biomaterials.2008.01.006.

[142] C.M. Murphy, M.G. Haugh, F.J. O'Brien, The effect of mean pore size on cell attachment, proliferation and migration in collagen-glycosaminoglycan scaffolds for bone tissue engineering, Biomaterials. 31 (2010) 461–466. doi:10.1016/j.biomaterials.2009.09.063.

[143] B. Tavsanli, O. Okay, Macroporous methacrylated hyaluronic acid cryogels of high mechanical strength and flow-dependent viscoelasticity, Carbohydr. Polym. 229 (2020) 115458. doi:10.1016/j.carbpol.2019.115458.

[144] I. Noshadi, S. Hong, K.E. Sullivan, E. Shirzaei Sani, R. Portillo-Lara, A. Tamayol, S.R. Shin, A.E. Gao, W.L. Stoppel, L.D. Black III, A. Khademhosseini, N. Annabi, In vitro and in vivo analysis of visible light crosslinkable gelatin methacryloyl (GelMA) hydrogels, Biomater. Sci. 5 (2017) 2093–2105. doi:10.1039/C7BM00110J.

[145] Z. Wang, H. Kumar, Z. Tian, X. Jin, J.F. Holzman, F. Menard, K. Kim, Visible Light Photoinitiation of Cell-Adhesive Gelatin Methacryloyl Hydrogels for Stereolithography 3D Bioprinting, ACS Appl. Mater. Interfaces. 10 (2018) 26859–26869. doi:10.1021/acsami.8b06607.

[146] Z. Wang, Development of a visible light stereolithography-based bioprinting system for tissue engineering, (2016). doi:10.14288/1.0303476.

[147] D. Petta, U. D'Amora, L. Ambrosio, D. Grijpma, D. Eglin, M. D'Este, Hyaluronic acid as a (bio)ink for extrusion-based 3D printing, Biofabrication. (2020). doi:10.1088/1758-5090/ab8752.